Synchronization in Complex Oscillator Networks: A Survey

Florian Dörfler [a], Francesco Bullo [a]

[a] *Center for Control, Dynamical Systems and Computation, University of California, Santa Barbara, USA*

Abstract

The emergence of synchronization in a network of coupled oscillators is a fascinating subject of multidisciplinary research. This survey reviews the vast literature on the theory and the applications of complex oscillator networks. We focus on the canonical phase oscillator model that is ubiquitous in real-world synchronization phenomena, that generalizes the celebrated Kuramoto model, and that features a rich phenomenology. We review the history and the countless applications of this model throughout science and engineering. We justify the importance of the canonical coupled oscillator model and describe some selected applications relevant to control scientists, including vehicle coordination, electric power networks, and clock synchronization. We introduce the reader to several synchronization notions and performance estimates. We propose analysis approaches to phase and frequency synchronization, phase balancing, pattern formation, and partial synchronization. We present the sharpest known results about synchronization in networks of homogeneous and heterogeneous oscillators, with complete or sparse interconnection topologies, and in finite-dimensional and infinite-dimensional settings. We conclude by summarizing the limitations of existing analysis methods and by highlighting some directions for future research.

1 Introduction

Synchronization in networks of coupled oscillators is a pervasive topic in various scientific disciplines ranging from biology, physics, and chemistry to social networks and technological applications. A coupled oscillator network is characterized by a population of heterogeneous oscillators and a graph describing the interaction among the oscillators. These two ingredients give rise to a rich dynamic behavior that keeps on fascinating the scientific community.

Within the rich modeling phenomenology on synchronization among coupled oscillators, this article focuses on the canonical model of a continuous-time limit-cycle oscillator network with continuous, bidirectional, and sinusoidal coupling. We consider a system of n oscillators, each characterized by a phase angle $\theta_i \in \mathbb{S}^1$ and a natural rotation frequency $\omega_i \in \mathbb{R}$. The dynamics of each isolated oscillator are thus $\dot{\theta}_i = \omega_i$ for $i \in \{1, \dots, n\}$. The interaction topology and coupling strength among the oscillators are modeled by a connected, undirected, and weighted graph $G = (\mathcal{V}, \mathcal{E}, A)$ with nodes $\mathcal{V} = \{1, \dots, n\}$, edges $\mathcal{E} \subset \mathcal{V} \times \mathcal{V}$, and positive weights $a_{ij} = a_{ji} > 0$ for each undirected edge $\{i, j\} \in \mathcal{E}$. The interaction between neighboring oscillators is assumed to be additive, anti-symmetric, diffusive, [1] and proportional to the coupling strengths a_{ij}. In this case, the simplest 2π-periodic interaction function between neighboring oscillators $\{i, j\} \in \mathcal{E}$ is $a_{ij} \sin(\theta_i - \theta_j)$, and the overall model of coupled oscillators reads

$$\dot{\theta}_i = \omega_i - \sum\nolimits_{j=1}^{n} a_{ij} \sin(\theta_i - \theta_j), \quad i \in \{1, \dots, n\}. \tag{1}$$

Despite its apparent simplicity, this coupled oscillator model gives rise to rich dynamic behavior, and it is encountered in ubiquitous scientific disciplines ranging from natural and life sciences to engineering. This article surveys recent results and applications of the coupled oscillator model (1) and of its variations.

The motivations for this survey are manifold. Recent years have witnessed much theoretical progress and

⋆ This material is based in part upon work supported by NSF grants IIS-0904501 and CPS-1135819. A preliminary short version of this document appeared as (Dörfler and Bullo, 2012a).

Email addresses: dorfler@engineering.ucsb.edu (Florian Dörfler), bullo@engineering.ucsb.edu (Francesco Bullo).

[1] The interaction between two oscillators is *diffusive* if its strength depends on the corresponding phase difference; such interactions arise for example in the discretization of the Laplace operator in diffusive partial differential equations.

novel applications, which are not covered in existing surveys (Strogatz, 2000; Acebrón et al., 2005; Arenas et al., 2008) published in the physics literature. Indeed, control scientists have shown an increasing interest in networks of coupled oscillators and have recently contributed novel approaches and results. Much of this interest has focused on (i) synchronization rather than more complex phenomena, (ii) finite numbers of oscillators with a non-trivial interaction topology, and (iii) connections with graph theory and multi-agent systems. It is therefore timely to provide a comprehensive review in a unified control-theoretical language of the best known results in this area. With this aim, this survey provides a systems and control perspective to coupled oscillator networks, focusing on quantitative results and control-relevant applications in sciences and technology.

1.1 *Mechanical Analog and Basic Phenomenology*

A mechanical analog of a coupled oscillator network is the spring network shown in Figure 1. This network consists of a group of kinematic particles constrained to move on a unit circle and assumed to move without colliding. Each particle is characterized by an angle $\theta_i \in \mathbb{S}^1$

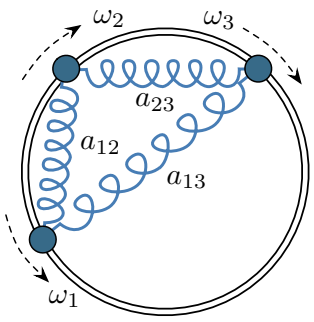

Fig. 1. Mechanical analog of a coupled oscillator network

and is subject to an external driving torque $\omega_i \in \mathbb{R}$. Pairs of interacting particles i and j are coupled through a linear-elastic spring with stiffness $a_{ij} > 0$. The overall spring network is modeled by a graph, whose nodes are the kinematic particles, whose edges are the linear-elastic springs, and whose edge weights are the positive stiffness coefficients $a_{ij} = a_{ji}$. Under these assumptions and by writing the mechanical system as a first-order vector field, it can be shown (Dörfler et al., 2013) that the system of spring-interconnected kinematic particles obeys the coupled oscillator dynamics (1).

The mechanical analog in Figure 1 illustrates the basic phenomenology displayed by the oscillator network (1). The spring-interconnected particles are subject to a competition between the external driving forces ω_i and the internal restoring torques $a_{ij}\sin(\theta_i - \theta_j)$. Hence, the interesting coupled oscillator dynamics (1) arise from a trade-off between each oscillator's tendency to align with its natural frequency ω_i and the synchronization-enforcing coupling $a_{ij}\sin(\theta_i - \theta_j)$ with its neighbors. Intuitively, a weakly coupled and strongly heterogeneous (i.e., with strongly dissimilar natural frequencies) network does not display any coherent behavior, whereas a strongly coupled and sufficiently homogeneous network is amenable to synchronization, where all frequencies $\dot{\theta}_i(t)$ or even all phases $\theta_i(t)$ become aligned.

1.2 *History, Related Applications, and Theoretical Developments:*

A brief historical account: The scientific interest in synchronization of coupled oscillators can be traced back to the work by Huygens (1893) on "an odd kind of sympathy" between coupled pendulum clocks, locking phenomena in circuits and radio technology (Adler, 1946), the analysis of brain waves and self-organizing systems (Wiener, 1948, 1958), and it still fascinates the scientific community nowadays (Winfree, 2001; Strogatz, 2003). A variation of the considered coupled oscillator model (1) was first proposed by Winfree (1967). Winfree considered general (not necessarily sinusoidal) interactions among the oscillators. He discovered a phase transition from incoherent behavior with dispersed phases to synchrony with aligned frequencies and coherent (i.e., nearby) phases. Winfree found that this phase transition depends on the trade-off between the heterogeneity of the oscillator population and the strength of the mutual coupling, which he could formulate by parametric thresholds. However, Winfree's model was too general to be analytically tractable. Inspired by these works, Kuramoto (1975) simplified Winfree's model and arrived at the coupled oscillator dynamics (1) with a complete interaction graph and uniform weights $a_{ij} = K/n$:

$$\dot{\theta}_i = \omega_i - \frac{K}{n}\sum_{j=1}^{n}\sin(\theta_i - \theta_j)\,, \qquad i \in \{1,\dots,n\}\,. \quad (2)$$

In an insightful and ingenious analysis, Kuramoto (1975, 1984a) showed that synchronization occurs in the model (2) if the coupling gain K exceeds a certain threshold K_{critical} function of the distribution of the natural frequencies ω_i. The dynamics (2) are nowadays known as the *Kuramoto model* of coupled oscillators, and Kuramoto's original work initiated a broad stream of research. A compelling historical perspective is offered by Strogatz (2000). We also recommend the surveys by Acebrón et al. (2005) and Arenas et al. (2008, Section 3).

Applications in sciences: The coupled oscillator model (1) and its variations appear in the study of biological synchronization and rhythmic phenomena. Example systems include pacemaker cells in the heart (Michaels et al., 1987), circadian cells in the brain (Liu et al., 1997), coupled cortical neurons (Crook et al., 1997), Hodgkin-Huxley neurons (Brown et al., 2003), brain networks (Varela et al., 2001), yeast cells (Ghosh

et al., 1971), flashing fireflies (Buck, 1988; Ermentrout, 1991), chirping crickets (Walker, 1969), central pattern generators for animal locomotion (Kopell and Ermentrout, 1988), particle models mimicking animal flocking behavior (Ha et al., 2010b, 2011), and fish schools (Paley et al., 2007), among others. The coupled oscillator model (1) also appears in physics and chemistry in modeling and analysis of spin glass models (Daido, 1992; Jongen et al., 2001), flavor evolution of neutrinos (Pantaleone, 1998), coupled Josephson junctions (Wiesenfeld et al., 1998), coupled metronomes (Pantaleone, 2002), Huygen's coupled pendulum clocks (Bennett et al., 2002; Kapitaniak et al., 2012), micromechanical oscillators with optical (Zhang et al., 2012) or mechanical (Shim et al., 2007) coupling, and in the analysis of chemical oscillations (Kuramoto, 1984a; Kiss et al., 2002). Finally, oscillator networks of the form (1) also serve as phenomenological models for synchronization phenomena in social networks, such as rhythmic applause (Néda et al., 2000), opinion dynamics (Pluchino et al., 2006a,b), pedestrian crowd synchrony on London's Millennium bridge (Strogatz et al., 2005), and decision making in animal groups (Leonard et al., 2012).

Applications in engineering: Some technological applications of the coupled oscillator model (1) include deep brain stimulation (Tass, 2003; Nabi and Moehlis, 2011), locking in solid-state circuit oscillators (Abidi and Chua, 1979; Mirzaei et al., 2007), planar vehicle coordination (Paley et al., 2007; Sepulchre et al., 2007, 2008; Klein, 2008; Klein et al., 2008), carrier synchronization without phase-locked loops (Rahman et al., 2011), synchronization in semiconductor laser arrays (Kozyreff et al., 2000), and microwave oscillator arrays (York and Compton, 2002). Since alternating current (AC) circuits are naturally modeled by equations similar to (1), some electric applications are found in structure-preserving (Bergen and Hill, 1981; Sauer and Pai, 1998) and network-reduced power system models (Chiang et al., 1995; Dörfler and Bullo, 2012b), and droop-controlled inverters in microgrids (Simpson-Porco et al., 2012). Algorithmic applications of the coupled oscillator model (1) include limit cycle estimation through particle filters (Tilton et al., 2012), clock synchronization in decentralized computing networks (Simeone et al., 2008; Baldoni et al., 2010; Wang et al., 2012), central pattern generators for robotic locomotion (Aoi and Tsuchiya, 2005; Righetti and Ijspeert, 2006; Ijspeert, 2008), decentralized maximum likelihood estimation (Barbarossa and Scutari, 2007), and human-robot interaction (Mizumoto et al., 2010). Further envisioned applications of oscillator networks obeying equations similar to (1) include generating music (Huepe et al., 2012), signal processing (Shim et al., 2007), and neuro-computing through micromechanical (Hoppensteadt and Izhikevich, 2001) or laser (Hoppensteadt and Izhikevich, 2000; Wang and Ghosh, 2007) oscillators.

Canonical model and prototypical example: The importance of the coupled oscillator model (1) does not stem only from the various examples listed above. Even though this model appears to be quite specific (a phase oscillator with constant driving term and diffusive sinusoidal coupling), it is the *canonical model* for coupled limit-cycle oscillators (Hoppensteadt and Izhikevich, 1997). This fact is established, for example, in work by the computational neuroscience community which has developed different approaches (Ermentrout and Kopell, 1984; Hoppensteadt and Izhikevich, 1997; Izhikevich and Kuramoto, 2006; Izhikevich, 2007) to reduce general oscillator and interaction models to phase oscillator networks of the form (1). Finally, the coupled oscillator model (1) serves as the prototypical example for synchronization in complex networks (Strogatz, 2001; Boccaletti et al., 2006; Osipov et al., 2007; Suykens and Osipov, 2008; Arenas et al., 2008), and its linearization is the well-known consensus protocol studied in networked control, see the surveys and monographs (Olfati-Saber et al., 2007; Ren et al., 2007; Bullo et al., 2009; Garin and Schenato, 2010; Mesbahi and Egerstedt, 2010). Indeed, numerous control scientists explored the coupled oscillator model (1) as a nonlinear generalization of the consensus protocol (Jadbabaie et al., 2004; Moreau, 2005; Scardovi et al., 2007; Olfati-Saber, 2006; Lin et al., 2007; Chopra and Spong, 2009; Sarlette and Sepulchre, 2009; Sepulchre, 2011).

Theoretical investigations: Coupled oscillator models of the form (1) are studied from a purely theoretical perspective in the physics, dynamical systems, and control communities. At the heart of the coupled oscillator dynamics is the transition from incoherence to synchrony. In this article we will be particularly interested in the notion of frequency synchronization, that is, in the property of certain solutions to reach equal frequencies $\dot{\theta}_i(t)$ among all oscillators. We will also study conditions under which the angles $\theta_i(t)$ themselves synchronize, or they are tightly clustered (in a single or multiple groups), or they are spread evenly in regular patterns over the circle. We refer to the surveys and tutorials (Kuramoto, 1984b; Strogatz, 2000, 2001; Acebrón et al., 2005; Boccaletti et al., 2006; Arenas et al., 2008; Dörfler and Bullo, 2011; Mauroy et al., 2012) for an incomplete set of recent theoretical research activities. We will review and attribute relevant theoretical results throughout the course of this paper.

1.3 Contributions and Contents:

This paper surveys the literature on synchronization in networks of coupled oscillators from a unified control-theoretical perspective. We present some selected applications relevant to control systems, we discuss a sample of important analysis methods based on control-theoretical concepts, and we provide a comprehensive review of the most-recent and sharpest results available for complex oscillator networks. For the sake of a clear

and streamlined presentation, we present some selected applications, analysis methods, and results in detail, and only list the corresponding references otherwise. Due to the limited space, we can review only a selected subset of the expansive literature on this subject.

In Section 2, we review some selected technological applications of the coupled oscillator model (1) which are relevant to control systems. We present in some detail various problems in vehicle coordination, electric power networks, and clock synchronization, and we justify the importance of the coupled oscillator model (1) as a canonical model.

Prompted by these applications, Section 3 introduces the reader to different synchronization notions, including frequency and phase synchronization, phase balancing, pattern formation, and partial synchronization. These notions are defined for finite and infinite oscillator populations, connected through complete or sparsely-coupled networks. We illustrate these concepts with a simple yet rich example that nicely explains the basic phenomenology in coupled oscillator networks.

Section 4 presents a few basic results and useful analysis methods, including studies on the Jacobian linearization of the dynamics (1), appropriate Lyapunov functions, and (incremental) boundedness. These basic results will be exploited throughout the rest of the paper.

Section 5 surveys a set of important results for networks of identical oscillators. In particular, we cover phase synchronization, phase balancing, and pattern formation. We highlight contraction properties and potential function arguments as powerful analysis methods.

Section 6 is devoted to complete and uniformly-weighted networks of heterogeneous oscillators, that is, the classic Kuramoto model (2). We cover both finite-dimensional as well as infinite-dimensional populations and present a set of necessary, sufficient, implicit, and explicit conditions on the critical coupling strength K_{critical}. In this effort, we collect contributions from several references and arrive at novel results within a unified perspective.

Section 7 surveys synchronization metrics, results, and analysis methods for sparse networks of heterogeneous oscillators. We present two sufficient conditions for synchronization. The first condition comes with an estimate of the region of attraction, whereas the second condition is sharper but the regions of attraction of the synchronized solution is unknown in this case. Since both conditions are conservative for general network topologies and parameters, we also present a recent analysis approach leading to a sharp sufficient condition for certain classes of oscillator networks.

In the final Section 8, we summarize the limitations of existing analysis methods and highlight some important directions for future research.

1.4 Preliminaries and Notation:

The remainder of this section recalls some standard notation and preliminaries from algebraic graph theory.

Vectors and functions: Let $\mathbf{1}_n$ and $\mathbf{0}_n$ be the n-dimensional vectors of unit and zero entries, and let $\mathbf{1}_n^\perp$ be the orthogonal complement of $\mathbf{1}_n$ in $\mathbb{R}^n$, that is, $\mathbf{1}_n^\perp \triangleq \{x \in \mathbb{R}^n \mid x \perp \mathbf{1}_n\}$. Accordingly, let $\mathbf{1}_{n\times n}$ denote the $(n \times n)$-dimensional matrix with unit entries. Given an n-tuple $(x_1, \dots, x_n)$, let $x \in \mathbb{R}^n$ be the associated vector with maximum and minimum elements $x_{\max}$ and $x_{\min}$. Given an ordered index set $\mathcal{I}$ of cardinality $|\mathcal{I}|$ and a one-dimensional array $\{x_i\}_{i\in\mathcal{I}}$, let $\operatorname{diag}(\{x_i\}_{i\in\mathcal{I}}) \in \mathbb{R}^{|\mathcal{I}|\times|\mathcal{I}|}$ be the associated diagonal matrix. For $x \in \mathbb{R}^n$ define $\mathbf{sin}(x) = (\sin(x_1), \dots, \sin(x_n))$ and for $x \in [-1, 1]^n$ define $\mathbf{arcsin}(x) = (\arcsin(x_1), \dots, \arcsin(x_n))$. Finally, define the continuous function $\operatorname{sinc} : \mathbb{R} \to \mathbb{R}$ by $\operatorname{sinc}(x) = \sin(x)/x$ for $x \neq 0$.

Geometry on the n-torus: The set $\mathbb{S}^1$ denotes the *unit circle*, an *angle* is a point $\theta \in \mathbb{S}^1$, and an *arc* is a connected subset of $\mathbb{S}^1$. The *n-torus* is the Cartesian product $\mathbb{T}^n = \mathbb{S}^1 \times \cdots \times \mathbb{S}^1$. The *geodesic distance* between two angles θ_1, θ_2 is the minimum of the counter-clockwise and the clockwise arc lengths connecting θ_1 and θ_2. With slight abuse of notation, let $|\theta_1 - \theta_2|$ denote the *geodesic distance* between the two angles $\theta_1, \theta_2 \in \mathbb{S}^1$.

Algebraic graph theory: Let $G(\mathcal{V}, \mathcal{E}, A)$ be an undirected, connected, and weighted graph without self-loops. Let $A \in \mathbb{R}^{n\times n}$ be its symmetric nonnegative *adjacency matrix* with zero diagonal elements $a_{ii} = 0$. For each node $i \in \{1, \dots, n\}$, define the node degree by $\deg_i = \sum_{j=1}^n a_{ij}$. Define the *Laplacian matrix* by $L = \operatorname{diag}(\{\deg_i\}_{i=1}^n) - A \in \mathbb{R}^{n\times n}$. If a unique number $\ell \in \{1, \dots, |\mathcal{E}|\}$ and an arbitrary direction are assigned to each edge $\{i, j\} \in \mathcal{E}$, the (oriented) *incidence matrix* $B \in \mathbb{R}^{n\times|\mathcal{E}|}$ is defined component-wise by $B_{k\ell} = 1$ if node k is the sink node of edge ℓ and by $B_{k\ell} = -1$ if node k is the source node of edge ℓ; all other elements are zero. For $x \in \mathbb{R}^n$, the vector $B^T x \in \mathbb{R}^{|\mathcal{E}|}$ has entries of the form $x_i - x_j$ corresponding to the oriented edge from j to i, that is, B^T maps node variables x_i, x_j to incremental edge variables $x_i - x_j$. If $\operatorname{diag}(\{a_{ij}\}_{\{i,j\}\in\mathcal{E}})$ is the diagonal matrix of edge weights, then one can show $L = B \operatorname{diag}(\{a_{ij}\}_{\{i,j\}\in\mathcal{E}})B^T$. If the graph is connected, then $\operatorname{Ker}(B^T) = \operatorname{Ker}(L) = \operatorname{span}(\mathbf{1}_n)$, all $n - 1$ non-zero eigenvalues of L are strictly positive, and the second-smallest eigenvalue $\lambda_2(L)$ is called the *algebraic connectivity* and is a spectral connectivity measure.

Since the Laplacian L is singular, we will use its *Moore-Penrose pseudo inverse* $L^\dagger$. If $V \in \mathbb{R}^{n\times n}$ is an orthonor-

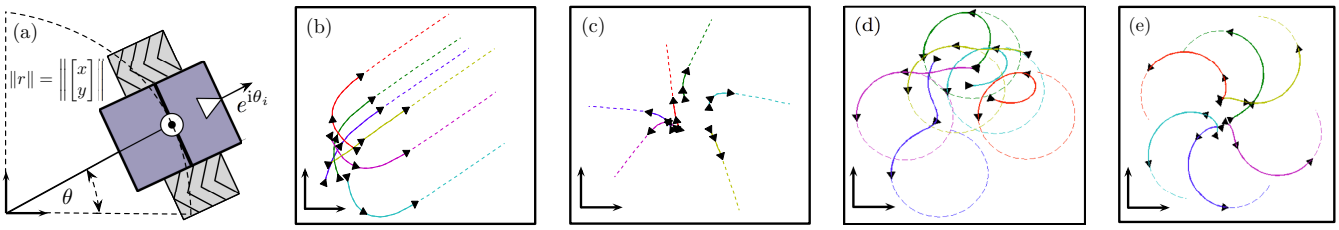

Fig. 2. Panel (a) illustrates the particle kinematics (4). Panels (b)-(e) illustrate the controlled dynamics (4)-(5) with $n=6$ particles, a complete interaction graph, and identical and constant natural frequencies: $\omega_0(t) = 0$ in panels (b) and (c) and $\omega_0(t) = 1$ in panels (d) and (e). The values of K are $K=1$ in panel (b) and (d) and $K=-1$ in panel (c) and (e). The arrows depict the orientation, the dashed curves show the long-term position dynamics, and the solid curves show the initial transient position dynamics. As illustrated, the resulting motion displays "synchronized" or "balanced" heading angles for $K = \pm 1$, and translational motion for $\omega_0(t) = 0$, respectively circular motion for $\omega_0(t) = 1$.

mal matrix of eigenvectors of L, the singular value decomposition of L is $L = V \operatorname{diag}(0, \{\lambda_i\}_{i\in\{2,\dots,n\}})V^T$, and its Moore-Penrose pseudo inverse $L^\dagger$ is given by $L^\dagger = V \operatorname{diag}(0, \{1/\lambda_i\}_{i\in\{2,\dots,n\}})V^T$. A direct consequence of the singular value decomposition is the identity $L \cdot L^\dagger = L^\dagger \cdot L = I_n - \frac{1}{n}\mathbf{1}_{n\times n}$. We also define the *effective resistance* between any two nodes i and j by $R_{ij} = L^\dagger_{ii} + L^\dagger_{jj} - 2L^\dagger_{ij}$. We refer to (Dörfler and Bullo, 2013) for further information and identities on Laplacian inverses and on the resistance distance

Laplacian flow: A well-studied cost function associated with a graph is the Laplacian potential $1/2 \cdot x^T L x = 1/2 \cdot \sum_{i,j=1}^n a_{ij}(x_i - x_j)^2$, defined for $x \in \mathbb{R}^n$. The associated gradient flow $\dot{x} = -Lx$ is known as the *Laplacian flow* or *consensus protocol*, and it reads in components as

$$\dot{x}_i = -\sum_{j=1}^n a_{ij}(x_i - x_j)\,. \tag{3}$$

The consensus protocol is well-studied in the control literature (Olfati-Saber et al., 2007; Ren et al., 2007; Bullo et al., 2009; Garin and Schenato, 2010; Mesbahi and Egerstedt, 2010), and it can be regarded as linear counterpart to the coupled oscillator model (1) with dynamics on Euclidean state space $\mathbb{R}^n$ and without drift terms. Some of the analysis tools and insights developed for the consensus protocol extend to the coupled oscillator model (1).

2 Selected Examples of Oscillator Networks Relevant to Control Systems

The mechanical analog in Figure 1 provides an intuitive illustration of the coupled oscillator dynamics (1), and Section 1 contains a survey of a wide range of applications. Here, we detail some selected exemplary applications, which have recently received significant attention by the control community, and we justify the importance of the oscillator network (1) as a canonical model.

2.1 Flocking, Schooling, and Vehicle Coordination

A recent research field in control is the coordination of autonomous vehicles based on locally available information and inspired by biological flocking phenomena. Consider a set of n particles in the plane $\mathbb{R}^2$, which we identify with the complex plane $\mathbb{C}$. Each particle $i \in \mathcal{V} = \{1, \dots, n\}$ is characterized by its position $r_i \in \mathbb{C}$, its heading angle $\theta_i \in \mathbb{S}^1$, and a steering control law $u_i(r, \theta)$ depending on the position and heading of itself and other vehicles, see Figure 2.(a). For simplicity, we assume that all particles have unit speed. The particle kinematics are then given by (Justh and Krishnaprasad, 2004)

$$\begin{aligned} \dot{r}_i &= e^{\mathrm{i}\theta_i}\,, \\ \dot{\theta}_i &= u_i(r, \theta)\,, \end{aligned} \tag{4}$$

for $i \in \{1, \dots, n\}$ and $\mathrm{i} = \sqrt{-1}$. If no control is applied, then particle i travels in a straight line with orientation $\theta_i(0)$, and if $u_i = \omega_i \in \mathbb{R}$ is a nonzero constant, then particle i traverses a circle with radius $1/|\omega_i|$.

The interaction among the particles is modeled by a possibly time-varying interaction graph $G(\mathcal{V}, \mathcal{E}(t), A(t))$ determined by communication and sensing patterns. Interesting motion patterns emerge if the controllers use only relative phase information between neighboring particles, that is, $u_i = \omega_0(t) + f_i(\theta_i - \theta_j)$ for $\{i, j\} \in \mathcal{E}(t)$ and $\omega_0 : \mathbb{R}_{\geq 0} \to \mathbb{R}$. For example, the steering control $u_i = \omega_0(t) - K \cdot \sum_{j=1}^n a_{ij}(t) \sin(\theta_i - \theta_j)$ with gain $K \in \mathbb{R}$ results in the phase dynamics

$$\dot{\theta}_i = \omega_0(t) - K \cdot \sum_{j=1}^n a_{ij}(t) \sin(\theta_i - \theta_j)\,, \quad i \in \mathcal{V}\,. \tag{5}$$

The controlled phase dynamics (5) correspond to the coupled oscillator model (1) with a time-varying interaction graph with weights $K \cdot a_{ij}(t)$ and identically time-varying natural frequencies $\omega_i = \omega_0(t)$. The controlled phase dynamics (5) give rise to elegant and useful coordination patterns that mimic animal flocking behavior (Leonard et al., 2012) and fish schools (Paley et al., 2007). A few representative trajectories are illustrated in

Figure 2. Inspired by these biological phenomena, scientists have studied the controlled phase dynamics (5) and their variations in the context of tracking and formation controllers in swarms of autonomous vehicles. We refer to (Paley et al., 2007; Sepulchre et al., 2007, 2008; Klein, 2008; Klein et al., 2008; Scardovi, 2010; Leonard et al., 2012) for other control laws, motion patterns, and their analysis.

In the following sections, we will present various tools to analyze the motion patterns in Figure 2, which we will refer to as *phase synchronization* (Figures 2.(b) and 2.(d)) and *phase balancing* (Figures 2.(c) and 2.(e)).

2.2 Electric Power Networks with Synchronous Generators and DC/AC Inverters

Consider an AC power network modeled as an undirected, connected, and weighted graph with n nodes $\mathcal{V} = \{1, \dots, n\}$, transmission lines $\mathcal{E} \subset \mathcal{V} \times \mathcal{V}$, and admittance matrix $Y = Y^T \in \mathbb{C}^{n \times n}$. For each node, consider the voltage phasor $V_i = |V_i| e^{\mathrm{i}\theta_i}$ corresponding to the phase $\theta_i \in \mathbb{S}^1$ and magnitude $|V_i| \geq 0$ of the sinusoidal solution to the circuit equations. If the network is lossless, then the active power flow from node i to j is $a_{ij} \sin(\theta_i - \theta_j)$, where we adopt the shorthand $a_{ij} = |V_i| \cdot |V_j| \cdot \Im(Y_{ij})$, see Figure 3.(a). The node set is partitioned as $\mathcal{V} = \mathcal{V}_1 \cup \mathcal{V}_2 \cup \mathcal{V}_3$, where $\mathcal{V}_1$ are load buses, $\mathcal{V}_2$ are synchronous generators, and $\mathcal{V}_3$ are grid-connected direct current (DC) power sources. The active power drawn by a load $i \in \mathcal{V}_1$ consists of a constant term $P_{\mathrm{l},i} > 0$ and a frequency-dependent term $D_i \dot{\theta}_i$ with $D_i > 0$, see Figure 3.(b). The resulting power balance equation is

$$D_i \dot{\theta}_i + P_{\mathrm{l},i} = -\sum_{j=1}^{n} a_{ij} \sin(\theta_i - \theta_j), \quad i \in \mathcal{V}_1 . \tag{6}$$

If the generator reactances are absorbed into the admittance matrix, then the swing dynamics of the synchronous generator $i \in \mathcal{V}_2$ are

$$M_i \ddot{\theta}_i + D_i \dot{\theta}_i = P_{\mathrm{m},i} - \sum_{j=1}^{n} a_{ij} \sin(\theta_i - \theta_j), \quad i \in \mathcal{V}_2, \tag{7}$$

where $\theta_i \in \mathbb{S}^1$ and $\dot{\theta}_i \in \mathbb{R}^1$ are the generator rotor angle and frequency, $P_{\mathrm{m},i} > 0$ is the mechanical power input, and $M_i > 0$, and $D_i > 0$ are the inertia and damping coefficients. The dynamics (6)-(7) constitute the *structure-preserving power network model*, proposed by Bergen and Hill (1981). A derivation from first principles can be found in (Sauer and Pai, 1998, Chapter 7).

We assume that each DC source is connected to the AC grid via a DC/AC inverter, the inverter output impedances are absorbed into the admittance matrix, and each inverter is equipped with a conventional droop controller. For a droop-controlled inverter $i \in \mathcal{V}_3$ with droop-slope $1/D_i > 0$, the deviation of the power output $\sum_{j=1}^{n} a_{ij} \sin(\theta_i - \theta_j)$ from its nominal value $P_{\mathrm{d},i} > 0$ is proportional to the frequency deviation $D_i \dot{\theta}_i$. This gives rise to the droop-controlled inverter dynamics (Simpson-Porco et al., 2012)

$$D_i \dot{\theta}_i = P_{\mathrm{d},i} - \sum_{j=1}^{n} a_{ij} \sin(\theta_i - \theta_j), \quad i \in \mathcal{V}_3 . \tag{8}$$

These power network devices are illustrated as circuit elements in panels (a)-(d) of Figure 3, and panels (e) and (f) show a high-voltage transmission network and a microgrid. Finally, we remark that different load models such as constant power/current/susceptance loads and synchronous motor loads can be modeled by the same set of equations (6)-(8), see (Sastry and Varaiya, 1980; Chiang et al., 1995; Sauer and Pai, 1998; Dörfler and Bullo, 2013).

Synchronization is pervasive in the operation of power networks. All generating units of an interconnected grid must remain in strict frequency synchronism while continuously following demand and rejecting disturbances. Notice that, with the exception of the inertial terms $M_i \ddot{\theta}_i$ and the possibly non-unit coefficients D_i, the power network dynamics (6)-(8) are a perfect electrical analog of the coupled oscillator model (1) with $\omega_i \in \{-P_{\mathrm{l},i}, P_{\mathrm{m},i}, P_{\mathrm{d},i}\}$. Thus, it is not surprising that scientists from different disciplines recently advocated coupled oscillator approaches to analyze synchronization in power networks (Tanaka et al., 1997; Subbarao et al., 2001; Hill and Chen, 2006; Filatrella et al., 2008; Buzna et al., 2009; Fioriti et al., 2009; Simpson-Porco et al., 2012; Dörfler and Bullo, 2012b; Rohden et al., 2012; Dörfler et al., 2013; Motter et al., 2013). The theoretical tools presented in this article establish how *frequency synchronization* in power networks depend on the nodal parameters $(P_{\mathrm{l},i}, P_{\mathrm{m},i}, P_{\mathrm{d},i})$ as well as the interconnecting electrical network with weights a_{ij}.

2.3 Clock Synchronization in Decentralized Networks

Another emerging technological application of oscillator networks is clock synchronization in decentralized computing networks, such as wireless and distributed software networks. A natural approach to clock synchronization is to treat each clock as an oscillator and follow a diffusion-based (or pulse-coupling) protocol to synchronize them, see the surveys (Lindsey et al., 1985; Simeone et al., 2008) and the interesting recent results (Hong and Scaglione, 2005; Baldoni et al., 2010; Mallada and Tang, 2011; Wang et al., 2012; Wang and Doyle, 2012).

For illustration, consider a set of distributed processors $\mathcal{V} = \{1, \dots, n\}$ connected by a (possibly directed) communication network. Each processor is equipped with an internal clock. These clocks need to be synchronized for distributed computing and network routing tasks. As

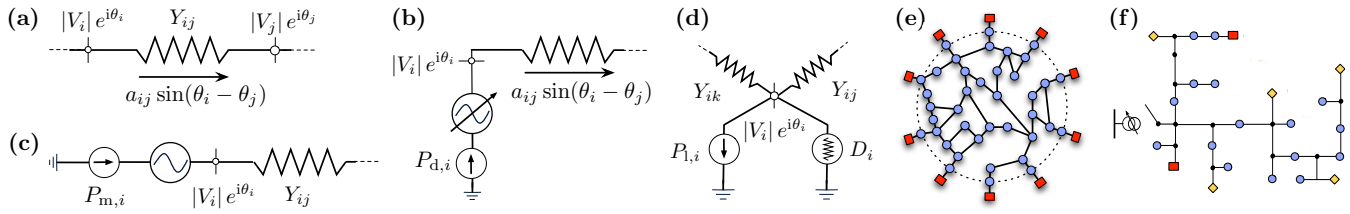

Fig. 3. Illustration of the power network devices as circuit elements. Subfigure (a) shows a transmission element connecting nodes i and j, Subfigure (b) shows an inverter controlled according to (8), Subfigure (c) shows a synchronous generator, and Subfigure (d) shows a frequency-dependent load. Subfigure (e) shows a schematic illustration of the IEEE 39 power grid, where the (red) squares depict synchronous generators and the (blue) circles are load buses. Finally, Subfigure (f) shows a microgrid based on the IEEE 37 feeder, where the (yellow) diamonds depict inverters and (black) circles are passive junctions.

discussed in the surveys (Lindsey et al., 1985; Simeone et al., 2008), we consider only analog clocks with continuous coupling since digital clocks are essentially discretized analog clocks, and pulse-coupled clocks can be modeled continuously after a phase reduction and averaging analysis. For our purposes, the clock of processor i is a voltage-controlled oscillator (VCO) generating a harmonic waveform $s_i(t) = \sin(\theta_i(t))$, where $\theta_i(t)$ is the accumulated instantaneous phase. For uncoupled clocks, each phase $\theta_i(t)$ evolves according to

$$\theta_i(t) = \left(\theta_i(0) + \frac{2\pi}{T_{\text{nom}} + T_i}t\right) \bmod (2\pi)\,,\ i \in \{1,\dots,n\}.$$

where $T_{\text{nom}} > 0$ is the nominal period, $T_i \in \mathbb{R}$ is an offset (or skew), and $\theta_i(0) \in \mathbb{S}^1$ is the initial phase. To synchronize their internal clocks, the processors follow a diffusion-based protocol. In a first step, neighboring oscillators communicate their respective waveforms $s_i(t)$ to another. Second, through a phase detector (PD) each node measures a convex combination of phase differences

$$\text{cvx}_i(\theta(t)) = \sum\nolimits_{j=1}^{n} a_{ij} f(\theta_i(t) - \theta_j(t))\,,\ i \in \{1,\dots,n\}\,,$$

where $f : \mathbb{S}^1 \to \mathbb{R}$ is an odd 2π-periodic function, and $a_{ij} \geq 0$ are detector-specific convex weights satisfying $\sum_{j=1}^{n} a_{ij} = 1$. Finally, $\text{cvx}_i(\theta(t))$ is fed to a phase-locked loop filter (PLL) whose output drives the local phase. A first-order and constant PLL with gain K results in

$$\dot\theta_i(t) = \frac{2\pi}{T_{\text{nom}} + T_i} + K \cdot \text{cvx}_i(\theta(t))\,,\quad i \in \{1,\dots,n\}\,. \quad (9)$$

The diffusion-based synchronization protocol (9) is illustrated in Figure 4, and its objective is to synchronize the frequencies $\dot\theta_i(t)$ and possibly also the phases $\theta_i(t)$ in the processor network. For an undirected communication protocol, symmetric weights $a_{ij} = a_{ji}$, and a sinusoidal coupling function $f(\cdot) = \sin(\cdot)$, the synchronization protocol (9) equals the coupled oscillator model (1).

The tools developed in the next section will enable us to state conditions when the protocol (9) successfully achieves phase or frequency synchronization. The

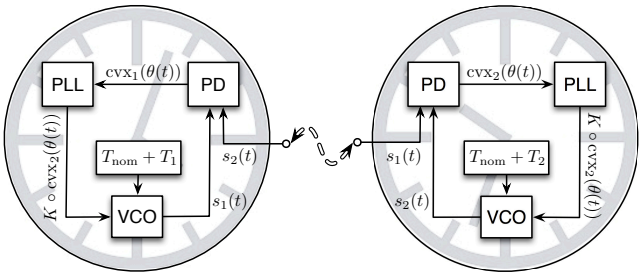

Fig. 4. Schematic illustration of the diffusion-based synchronization protocol (9) for two coupled analog clocks.

protocol (9) is merely a starting point, more sophisticated higher-order PLLs can be constructed to enhance steady-state deviations from phase synchrony, communication and phase noise as well as time-delays can be considered in the design, and the phase coupling functions f can be optimized to increase the synchronization rate or minimize energy consumption.

2.4 Canonical Coupled Oscillator Model

In the preceeding subsections we have seen how the coupled-oscillator model (1) appears naturally in various applications. We now illustrate how this apparently-specific model is known as the *canonical model* of coupled limit-cycle oscillators (Hoppensteadt and Izhikevich, 1997) and is obtained through a standard reduction procedure from general limit-cycle oscillator and interaction models. Our presentation is informal, we schematically follow the approaches developed in the computational neuroscience community, and we refer to the textbooks (Hoppensteadt and Izhikevich, 1997; Izhikevich, 2007), the tutorials (Izhikevich and Kuramoto, 2006; Mauroy et al., 2012), and the pioneering papers (Winfree, 1967; Ermentrout and Kopell, 1984) for further details.

Consider a limit-cycle oscillator modeled as a dynamical system with state $x \in \mathbb{R}^m$ and nonlinear dynamics $\dot x = f(x)$. Assume that this system admits a locally exponentially stable periodic orbit $\mathcal{S} \subset \mathbb{R}^m$ with period $T > 0$. By a local change of variables, any trajectory in a neighborhood of $\mathcal{S}$ can be characterized by a phase variable $\varphi \in \mathbb{S}^1$ with dynamics $\dot\varphi = \Omega$, where $\Omega = 2\pi/T$.

Now consider a weakly-forced oscillator of the form

$$\dot{x}(t) = f(x(t)) + \epsilon g(t)\,, \tag{10}$$

where $\epsilon > 0$ is sufficiently small and $g(t)$ is a time-dependent external forcing term. For sufficiently small forcing $\epsilon g(t)$, the attractive limit cycle $\mathcal{S}$ persists, and the local phase dynamics are obtained as

$$\dot{\varphi}(t) = \Omega + \epsilon Q(\varphi(t))g(t)\,,$$

where $\varphi \mapsto Q(\varphi)$ is the *infinitesimal phase response curve* (iPRC) and we dropped higher order terms $\mathcal{O}(\epsilon^2)$. The iPRC is a linear response function that associates to each point on the periodic orbit $\mathcal{S}$ (parameterized by the phase φ) the phase shift induced by the input $\epsilon g(t)$.

Now consider n such limit-cycle oscillators. Let $x_i \in \mathbb{R}^m$ be the state of oscillator i with limit cycle $\mathcal{S}_i \subset \mathbb{R}^m$ and period $T_i > 0$. We assume that the oscillators are weakly coupled with interaction graph $G(\mathcal{V}, \mathcal{E})$ and dynamics

$$\dot{x}_i = f_i(x_i) + \epsilon \sum\nolimits_{\{i,j\}\in\mathcal{E}} g_{ij}(x_i, x_j)\,, \quad i \in \{1, \dots, n\}\,, \tag{11}$$

where g_{ij} is the coupling function for the pair $\{i, j\} \in \mathcal{E}$. This coupling function may be continuous or impulsive. The weak coupling in (11) can be identified with the weak forcing in (10), and a transformation to phase coordinates yields

$$\dot{\varphi}_i = \Omega_i + \epsilon \sum\nolimits_{\{i,j\}\in\mathcal{E}} Q_i(\varphi_i) g_{ij}(x_i(\varphi_i), x_j(\varphi_j))\,,$$

where $\Omega_i = 2\pi/T_i$. The local change of variables $\theta_i(t) = \varphi_i(t) - \Omega_i t$ then yields the coupled phase dynamics

$$\dot{\theta}_i = \epsilon \sum\nolimits_{\{i,j\}\in\mathcal{E}} Q_i(\theta_i{+}\Omega_i t) g_{ij}(x_i(\theta_i{+}\Omega_i t), x_j(\theta_j{+}\Omega_j t))\,.$$

An averaging analysis applied to the θ-dynamics yields

$$\dot{\theta}_i = \epsilon\omega_i + \epsilon \sum\nolimits_{\{i,j\}\in\mathcal{E}} h_{ij}(\theta_i - \theta_j)\,, \tag{12}$$

where the averaged coupling functions h_{ij} are

$$h_{ij}(\chi) = \lim_{T\to\infty} \frac{1}{T} \int_0^T Q_i(\Omega_i\tau) g_{ij}(x_i(\Omega_i\tau), x_j(\Omega_j\tau - \chi)) d\tau,$$

and $\omega_i = h_{ii}(0)$. Notice that the averaged coupling functions h_{ij} are 2π-periodic and the coupling in (12) is diffusive. If the interaction among the oscillators is anti-symmetric, then all functions h_{ij} are odd, and a first-order Fourier series expansion yields $h_{ij}(\cdot) \approx a_{ij}\sin(\cdot)$ as first harmonic with coefficient a_{ij}. In this case, the dynamics (12) in the slow time scale $\tau = \epsilon t$ reduce exactly to the coupled oscillator model (1). This analysis justifies calling the coupled oscillator model (1) the *canonical model* for coupled limit-cycle oscillators. It also explains the widespread adoption of the oscillator network (1) as phenomenological model in synchronization studies.

For example, for two coupled van der Pol oscillators (with parameters in the quasi-harmonic limit) the above procedure results exactly in the coupled oscillator model (1), see the analysis by Mauroy et al. (2012). In general, the coupling functions h_{ij} depend on the iPRC and may not be sinusoidal. Hence, the iPRC serves as a natural analysis (Sacré and Sepulchre, 2012; Brown et al., 2004) and design (Wang et al., 2012; Wang and Doyle, 2012) tool for general limit-cycle oscillator models.

3 Synchronization Notions and Metrics

In this section, we introduce different notions of synchronization illustrated in Figure 5. We first address various commonly-studied notions of synchronization associated with coherent behavior and cohesive phases. We then address the concept of phase balancing and splay states. Finally, we discuss the setting of infinite-dimensional systems.

3.1 Synchronization Notions

The coupled oscillator model (1) evolves on $\mathbb{T}^n$ and features an important symmetry, namely, the rotational invariance of the angular variable θ. This symmetry gives rise to the structure of the state space and the different synchronization properties that the model (1) can display. All notions of synchronized solutions share the common property that the frequencies are equal to a constant synchronization frequency.

Frequency synchronization: A solution $\theta : \mathbb{R}_{\geq 0} \to \mathbb{T}^n$ achieves *frequency synchronization* if all frequencies $\dot{\theta}_i(t)$ converge to a common constant frequency $\omega_{\text{sync}} \in \mathbb{R}$ as $t \to \infty$. The explicit synchronization frequency $\omega_{\text{sync}} \in \mathbb{R}$ of the coupled oscillator model (1) can be obtained by summing over all equations in (1) as $\sum_{i=1}^n \dot{\theta}_i = \sum_{i=1}^n \omega_i$. In the frequency-synchronized case, this sum simplifies to $\sum_{i=1}^n \omega_{\text{sync}} = \sum_{i=1}^n \omega_i$. In conclusion, if a solution of the coupled oscillator model (1) achieves frequency synchronization, then it does so with synchronization frequency equal to $\omega_{\text{sync}} = \sum_{i=1}^n \omega_i/n$. By transforming to a rotating frame with frequency ω_{sync} and by replacing ω_i with $\omega_i - \omega_{\text{sync}}$, we obtain $\omega_{\text{sync}} = 0$ (or, equivalently, $\omega \in \mathbf{1}_n^\perp$). In what follows, without loss of generality, we assume that $\omega \in \mathbf{1}_n^\perp$ so that $\omega_{\text{sync}} = 0$.

Phase synchronization: A solution $\theta : \mathbb{R}_{\geq 0} \to \mathbb{T}^n$ to the coupled oscillator model (1) achieves *phase synchronization* if all phases $\theta_i(t)$ become identical as $t \to \infty$.

Remark 1 (Terminology) *Alternative terminologies for phase synchronization include full, exact, or perfect*

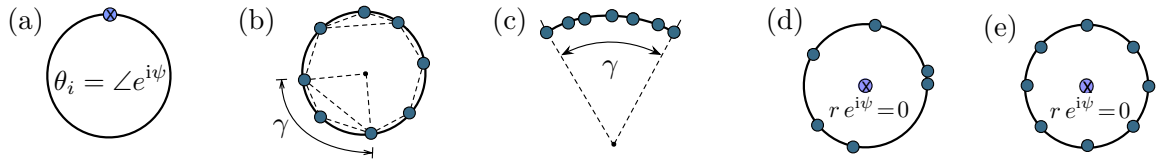

Fig. 5. Different phase configurations exhibited by frequency-synchronized solutions of the oscillator network (1): (a) phase synchronization, (b) phase cohesiveness, (c) arc invariance, (d) phase balancing, and (e) splay state synchronization.

synchronization. For a frequency-synchronized solution all phase distances $|\theta_i(t) - \theta_j(t)|$ are constant in a rotating coordinate frame with frequency ω_{sync}, and the terminology phase locking is sometimes used instead of frequency synchronization. Other commonly used terms instead of frequency synchronization include frequency locking, frequency entrainment, or also partial synchronization. □

Phase cohesiveness: As we will see later, phase synchronization can occur only if all natural frequencies ω_i are identical. If the natural frequencies are not identical, then each pairwise distance $|\theta_i(t) - \theta_j(t)|$ can converge to a constant but not necessarily zero value. The concept of phase cohesiveness formalizes this possibility. For $\gamma \in [0, \pi[$, let $\bar{\Delta}_G(\gamma) \subset \mathbb{T}^n$ be the closed set of angle arrays $(\theta_1, \dots, \theta_n)$ with the property $|\theta_i - \theta_j| \leq \gamma$ for all $\{i, j\} \in \mathcal{E}$, that is, each pairwise phase distance is upper bounded by γ. Also, let $\Delta_G(\gamma)$ be the interior of $\bar{\Delta}_G(\gamma)$. A solution $\theta : \mathbb{R}_{\geq 0} \to \mathbb{T}^n$ is then said to be *phase cohesive* if there exists a length $\gamma \in [0, \pi[$ such that $\theta(t) \in \bar{\Delta}_G(\gamma)$ for all $t \geq 0$. Notice that a phase cohesive solution is also phase synchronous when $\gamma = 0$.

The main object under study in most applications and theoretic analyses are phase-cohesive and frequency-synchronized solutions, where all oscillators rotate with the same frequency and all the pairwise phase distances are upper bounded. In the following, we restrict our attention to synchronized solutions with sufficiently small phase distances $|\theta_i - \theta_j| \leq \gamma < \pi/2$ for $\{i, j\} \in \mathcal{E}$. Of course, there may exist other synchronized solutions with larger phase distances, but these are not necessarily stable (see our analysis in Section 4) and/or not relevant in most applications. [2] In what follows, in the interest of brevity, we call a solution *synchronized* if it is frequency synchronized and phase cohesive.

Synchronization manifold: A geometric object of interest is the synchronization manifold. Given a point $r \in \mathbb{S}^1$ and an angle $s \in [0, 2\pi]$, let $\mathrm{rot}_s(r) \in \mathbb{S}^1$ be the rotation of r counterclockwise by the angle s. For $(r_1, \dots, r_n) \in \mathbb{T}^n$, define the equivalence class

$$[(r_1, \dots, r_n)] = \{(\mathrm{rot}_s(r_1), \dots, \mathrm{rot}_s(r_n)) \in \mathbb{T}^n \,|\, s \in [0, 2\pi]\}.$$

Clearly, if $(r_1, \dots, r_n) \in \bar{\Delta}_G(\gamma)$ for some $\gamma \in [0, \pi/2[$, then $[(r_1, \dots, r_n)] \subset \bar{\Delta}_G(\gamma)$. Given a synchronized solution characterized by $\theta_{\mathrm{sync}} \in \bar{\Delta}_G(\gamma)$ for some $\gamma \in [0, \pi/2[$, the set $[\theta_{\mathrm{sync}}] \subset \bar{\Delta}_G(\gamma)$ is a *synchronization manifold* of the coupled-oscillator model (1). Note that a synchronized solution takes value in a synchronization manifold due to rotational symmetry, and for $\omega \in \mathbf{1}_n^\perp$ (implying $\omega_{\mathrm{sync}} = 0$) a synchronization manifold is also an equilibrium manifold of the coupled oscillator model (1). These geometric concepts are illustrated in Figure 6 for the two-dimensional case.

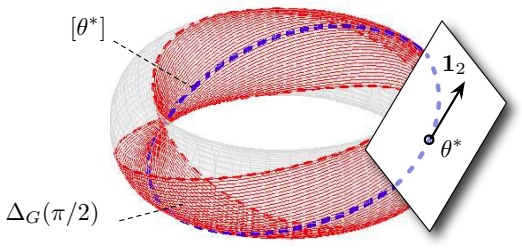

Fig. 6. Illustration of the state space $\mathbb{T}^2$, the set $\Delta_G(\pi/2)$, the synchronization manifold $[\theta^*]$ associated to a phase-synchronized angle array $\theta^* = (\theta_1^*, \theta_2^*) \in \bar{\Delta}_G(0)$, and the tangent space with translation vector $\mathbf{1}_2$ at θ^*.

Arc invariance: To conclude our list of synchronization notions, we introduce the concept of arc invariance. For $\gamma \in [0, 2\pi[$, let $\overline{\mathrm{Arc}}_n(\gamma) \subset \mathbb{T}^n$ be the closed set of angle arrays $\theta = (\theta_1, \dots, \theta_n)$ with the property that there exists an arc of length γ containing all $\theta_1, \dots, \theta_n$. Thus, an angle array $\theta \in \overline{\mathrm{Arc}}_n(\gamma)$ satisfies $\max_{i,j \in \{1,\dots,n\}} |\theta_i - \theta_j| \leq \gamma$. Finally, let $\mathrm{Arc}_n(\gamma)$ be the interior of the set $\overline{\mathrm{Arc}}_n(\gamma)$. A solution $\theta : \mathbb{R}_{\geq 0} \to \mathbb{T}^n$ is then said to be *arc invariant* if there exists a length $\gamma \in [0, 2\pi[$ such that $\theta(t) \in \overline{\mathrm{Arc}}_n(\gamma)$ for all $t \geq 0$. Notice that $\overline{\mathrm{Arc}}_n(\gamma) \subseteq \bar{\Delta}_G(\gamma)$ but the two sets are generally not equal. For a complete coupling graph, sufficiently many oscillators, and for sufficiently small γ, the two sets become equal, and arc invariance is an appropriate synchronization notion, see, e.g., Theorems 5.2 and 6.6.

[2] For example, in power network applications the coupling terms $a_{ij} \sin(\theta_i - \theta_j)$ are power flows along transmission lines $\{i, j\} \in \mathcal{E}$, and the phase distances $|\theta_i - \theta_j|$ are bounded well below $\pi/2$ due to thermal constraints. In Subsection 3.4, we present a converse synchronization notion termed phase balancing, where the goal is to maximize phase distances.

3.2 A Simple yet Illustrative Example

The following example illustrates different notions of synchronization and points out various important geometric subtleties occurring on the compact state space $\mathbb{T}^2$. Consider $n = 2$ oscillators with $\omega_2 \geq 0 \geq \omega_1 = -\omega_2$. We restrict our attention to angles contained in $\mathrm{Arc}_n(\pi)$: for angles θ_1, θ_2 with $|\theta_2 - \theta_1| < \pi$, the *angular difference* $\theta_2 - \theta_1$ is the number in $]-\pi, \pi[$ with magnitude equal to the geodesic distance $|\theta_2 - \theta_1|$ and with positive sign if and only if the counter-clockwise path length from θ_1 to θ_2 is smaller than the clockwise path length. With this definition the two-dimensional oscillator dynamics $(\dot\theta_1, \dot\theta_2)$ can be reduced to the scalar difference dynamics $\dot\theta_2 - \dot\theta_1$. After scaling time as $t \mapsto t(\omega_2 - \omega_1)$ and introducing $\kappa = 2a_{12}/(\omega_2 - \omega_1)$, the difference dynamics are

$$\frac{d}{dt}(\theta_2 - \theta_1) = f_\kappa(\theta_2 - \theta_1) \triangleq 1 - \kappa \sin(\theta_2 - \theta_1)\,. \quad (13)$$

The dynamics (13) can be analyzed graphically by plotting the scalar vector field $f_\kappa(\theta_2 - \theta_1)$, for $\theta_2 - \theta_1 \in [0, \pi]$, see Figure 7(a). Figure 7(a) displays a saddle-node bifurcation at $\kappa = 1$. For $\kappa < 1$ no equilibria exist. For $\kappa > 1$ we have an asymptotically stable equilibrium $\theta_{\text{stable}} = \arcsin(\kappa^{-1}) \in]0, \pi/2[$ together with an unstable equilibrium $\theta_{\text{unstable}} = \arcsin(\kappa^{-1}) \in]\pi/2, \pi[$. For $\kappa > 1$ and $\theta(0) \in [0, \theta_{\text{unstable}}[$, all trajectories converge to θ_{stable}, that is, the oscillators synchronize and remain phase cohesive (or arc invariant). For $\theta(0) \notin [0, \theta_{\text{unstable}}]$ the difference $\theta_2(t) - \theta_1(t)$ increases beyond π, and $\theta_2(t) - \theta_1(t)$ converges asymptotically to the equilibrium θ_{stable} in the set where $\theta_2 - \theta_1 < 0$. Equivalently in the configuration space $\mathbb{S}^1$, the oscillators revolve once around the circle before converging to $[\theta_{\text{stable}}]$. Since $\sin(\theta_{\text{stable}}) = \sin(\theta_{\text{unstable}}) = \kappa^{-1}$, in the limit $\kappa \to \infty$ the oscillators achieve phase synchronization from every initial condition in an open semi-circle $\mathrm{Arc}_2(\pi)$. In the critical case, $\kappa = 1$, the saddle equilibrium manifold at $[\theta_{\text{saddle}}]$ is globally attractive but not stable, see the trajectory in Figure 7(b).

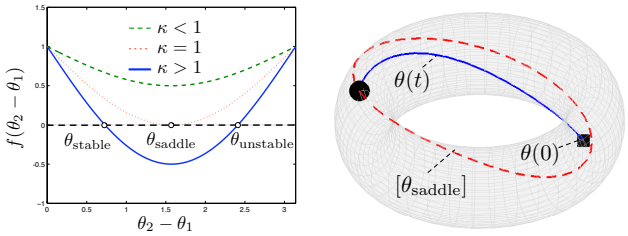

(a) Vector field in eq. (13) (b) Trajectory $\theta(t)$ for $\kappa = 1$

Fig. 7. Plot of the vector field (13) for $\theta_2 - \theta_1 > 0$ and various values of κ and a trajectory $\theta(t) \in \mathbb{T}^2$ for the critical case $\kappa = 1$, where the dashed line is the saddle equilibrium manifold and ■ and ● depict $\theta(0)$ and $\lim_{t\to\infty} \theta(t)$.

In conclusion, the simple but already rich 2-dimensional case shows that two oscillators are phase cohesive and synchronize if and only if $\kappa > 1$, that is, if and only if the coupling dominates the heterogeneity as $2a_{12} > \omega_2 - \omega_1$. The ratio $1/\kappa$ determines the asymptotic phase cohesiveness as well as the set of admissible initial conditions. More general oscillator networks display the same phenomenology, but the threshold from incoherence to synchrony is generally unknown. Finally, we remark that for oscillator networks of dimension $n \geq 3$, this loss of synchrony via a saddle-node bifurcation is only the starting point of a series of bifurcations occurring if the coupling is further decreased, see (Maistrenko et al., 2005; Tönjes, 2007; Popovych et al., 2005; Suykens and Osipov, 2008).

3.3 Synchronization Metrics

The notions of phase cohesiveness and arc invariance are performance measures for synchronization, and phase synchronization is the extreme case of phase cohesiveness with $\lim_{t\to\infty} \theta(t) \in \bar\Delta_G(0) = \overline{\mathrm{Arc}}_n(0)$. An alternative performance measure is the magnitude of the so-called *order parameter* introduced by Kuramoto (1975, 1984a) as

$$re^{\mathrm{i}\psi} = \frac{1}{n}\sum_{j=1}^{n} e^{\mathrm{i}\theta_j}\,. \quad (14)$$

The order parameter (14) is the centroid of all oscillators represented as points on the unit circle in $\mathbb{C}^1$. The magnitude r of the order parameter is a synchronization measure: if the oscillators are phase-synchronized, then $r = 1$, and if the oscillators are spaced equally on the unit circle, then $r = 0$, see Figure 5(e). The latter case is characterized in detail Subsection 3.4. Because the order parameter (14) is the centroid of the oscillators, it is contained within the convex hull of the smallest arc containing all oscillators, see the illustration in Figure 8. Hence, the magnitude r of the order parameter can be related to the arc length γ as in the following lemma.

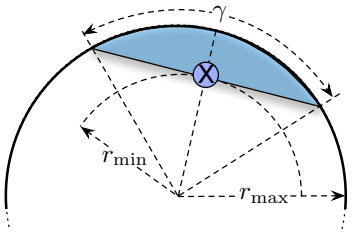

Fig. 8. Schematic illustration of an arc of length $\gamma \in [0, \pi]$, its convex hull (shaded), and the value ⊗ of the corresponding order parameter $re^{\mathrm{i}\psi}$ with minimum magnitude $r_{\text{min}} = \cos(\gamma/2)$ and maximum magnitude $r_{\text{max}} = 1$.

Lemma 3.1 (Shortest arc length and order parameter) *Given an angle array $\theta = (\theta_1, \ldots, \theta_n) \in \mathbb{T}^n$ with $n \geq 2$, let $r(\theta) = \frac{1}{n}|\sum_{j=1}^n e^{\mathrm{i}\theta_j}|$ be the magnitude of the order parameter, and let $\gamma(\theta)$ be the length of the shortest arc containing all angles, that is, $\theta \in \overline{\mathrm{Arc}}_n(\gamma(\theta))$. The following statements hold:*

1) if $\gamma(\theta) \in [0, \pi]$, then $r(\theta) \in [\cos(\gamma(\theta)/2), 1]$; and

2) if $\theta \in \overline{\mathrm{Arc}}_n(\pi)$*, then* $\gamma(\theta) \in [2\arccos(r(\theta)), \pi]$.

For a complete graph, the asymptotic magnitude r of the order parameter serves as an *average* performance index for synchronization, and arc invariance can be understood as a *worst-case* performance index. Appropriate definitions of the order parameter tailored to non-complete graphs have been proposed, among others, by Jadbabaie et al. (2004); Restrepo et al. (2005); Scardovi et al. (2007); Paley et al. (2007).

3.4 Phase Balancing, Splay State, and Patterns

Applications in neuroscience (Crook et al., 1997; Varela et al., 2001; Brown et al., 2003), deep-brain stimulation (Tass, 2003; Nabi and Moehlis, 2011), vehicle coordination (Paley et al., 2007; Sepulchre et al., 2007, 2008; Klein, 2008; Klein et al., 2008), and central pattern generators for locomotion purposes (Ijspeert, 2008; Aoi and Tsuchiya, 2005; Righetti and Ijspeert, 2006) motivate the study of coherent behaviors with synchronized frequencies where the phases are not cohesive, but rather dispersed in appropriate patterns. Whereas the phase-synchronized state is characterized by the order parameter r achieving its maximal (unit) magnitude, we say that a solution $\theta : \mathbb{R}_{\geq 0} \to \mathbb{T}^n$ to the coupled oscillator model (1) achieves *phase balancing* if all phases $\theta_i(t)$ asymptotically converge to

$$\mathrm{Bal}_n = \left\{ \theta \in \mathbb{T}^n \;\middle|\; r(\theta) = \left| \sum_{j=1}^{n} e^{\mathrm{i}\theta_j}/n \right| = 0 \right\},$$

that is, asymptotically the oscillators are uniformly distributed over the unit circle $\mathbb{S}^1$ so that their centroid converges to the origin; see Figure 5(d) and 5(e) for illustrations. We refer to Sepulchre et al. (2007) for a geometric characterization of the balanced state. One balanced state of particular interest in neuroscience applications is the so-called *splay state* $\{\theta \in \mathbb{T}^n \mid \theta_i = i \cdot 2\pi/n + \varphi \pmod{2\pi}, \varphi \in \mathbb{S}^1, i \in \{1, \dots, n\}\} \subseteq \mathrm{Bal}_n$ corresponding to phases uniformly distributed around the unit circle $\mathbb{S}^1$ with distances $2\pi/n$, see Figure 5(e).

Other highly-symmetric balanced states consist of multiple clusters of collocated oscillators, where the clusters themselves are arranged in splay state. In particular, if m is a divisor of n, we define a *symmetric balanced* (m, n)*-pattern* to be a symmetric arrangement of the n phases consisting of m clusters uniformly spaced on $\mathbb{S}^1$, where each cluster contains n/m synchronized phases. Figure 9 illustrates all symmetric balanced (m, n)-patterns for $n = 12$. Notice that, for any $n \in \mathbb{N}$, there are at least two symmetric patterns: the $(1, n)$-pattern (i.e., the phase-synchronized state) and the (n, n)-pattern (i.e., the splay state). Arbitrary (m, n)-patterns can be stabilized, for example, by using coupling functions with higher harmonics, such as $\sin(m(\theta_i - \theta_j))$; see (Sepulchre et al., 2007, 2008). The topic of symmetric phase balancing is similar in spirit to pattern formation (Cross and Hohenberg, 1993; Arcak, 2012), where phase synchronization corresponds to the "flat" solution with uniform phases and balanced (m, n)-patterns correspond to spatially non-uniform solutions with "higher-order modes."

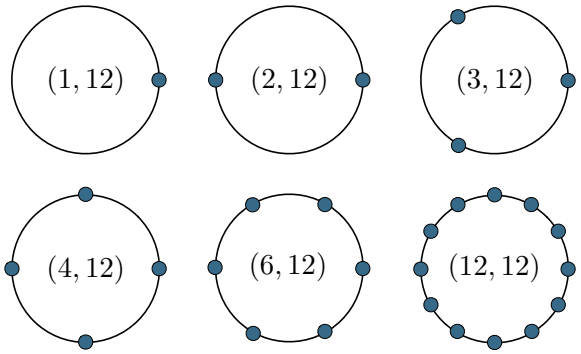

Fig. 9. Illustration of all symmetric balanced (m, n)-patterns for $n = 12$. The $(1, 12)$-pattern equals phase synchronization with $r = 1$, all other patterns are phase-balanced configurations with $r = 0$, and the $(12, 12)$-pattern is the splay state.

3.5 Synchronization in Infinite-Dimensional Networks

For a complete coupling graph with uniform weights $a_{ij} = K/n$, where $K > 0$, the coupled oscillator model (1) reduces to the celebrated Kuramoto model given in (2). By means of the order parameter $re^{\mathrm{i}\psi}$ defined in equation (14), the Kuramoto model (2) can be rewritten in the insightful form

$$\dot{\theta}_i = \omega_i - Kr\sin(\theta_i - \psi), \quad i \in \{1, \dots, n\}. \tag{15}$$

Equation (15) gives the intuition that the oscillators synchronize because of their coupling to a *mean field* represented by the order parameter $re^{\mathrm{i}\psi}$, which itself is a function of $\theta(t)$. Intuitively, for small coupling strength K each oscillator rotates with its distinct natural frequency ω_i, whereas for large coupling strength K all angles $\theta_i(t)$ will entrain to the mean field $re^{\mathrm{i}\psi}$, and the oscillators synchronize. The transition from incoherence to synchronization occurs at a critical threshold value of the coupling strength, denoted by K_{critical}.

The analysis of this phase transition based on a mean-field and statistical mechanics viewpoint has been the subject of numerous investigations, starting with Kuramoto's own ingenious analysis in (Kuramoto, 1975, 1984a). As neatly described by Strogatz (2000), Kuramoto assumed the a priori existence of solutions to (15) which feature a stationary order parameter $r(t)e^{\mathrm{i}\psi(t)} =$ constant. Following this assumption and his intuition, Kuramoto derived a set of self-consistency equations. A rigorous mathematical underpinning to Kuramoto's mean-field approach can be established by a time-scale separation (Ha and Slemrod, 2011) or in the continuum limit as the number of oscillators tends to infinity,

and the natural frequencies ω are sampled from a distribution function $g : \mathbb{R} \to \mathbb{R}_{\geq 0}$. The continuum-limit model has enjoyed a considerable amount of attention by the physics and dynamics communities. Related control-theoretical applications of the continuum limit can be found in (Yin et al., 2012; Tilton et al., 2012).

Continuum-limit model: Since infinite-dimensional oscillator networks are surveyed in detail in (Strogatz, 2000; Acebrón et al., 2005; Balmforth and Sassi, 2000), this paper discusses them only very briefly. In what follows, we present an informal Eulerian derivation of the continuum-limit model. We also remark that a treatment of (15) as a stochastic differential equation (in the limit of zero additive white noise) results in a Fokker-Planck equation analogous to the continuum-limit model (Crawford, 1994; Strogatz, 2000; Acebrón et al., 2005). Consider an infinite population of oscillators, and let $\rho : \mathbb{S}^1 \times \mathbb{R}_{\geq 0} \times \mathbb{R} \to \mathbb{R}_{\geq 0}$ be the probability density function of the oscillators, that is, $\int_0^\gamma \int_{\underline{\omega}}^{\overline{\omega}} \rho(\theta, t, \omega) g(\omega)\, d\omega d\theta$ denotes the fraction of oscillators in $\overline{\mathrm{Arc}}_n(\gamma) \subseteq \mathbb{S}^1$, at time t, and with frequencies $\omega \in [\underline{\omega}, \overline{\omega}]$. Hence, the order parameter is given by

$$r(t)e^{\mathrm{i}\psi(t)} = \int_0^{2\pi} \int_{-\infty}^{\infty} e^{\mathrm{i}\theta} \rho(\theta, t, \omega) g(\omega)\, d\omega d\theta. \qquad (16)$$

Notice that in the discrete (finite-dimensional) case $\rho(\theta, t, \omega) = \frac{1}{n} \sum_{j=1}^n \delta(\theta - \theta_j)$ (where $\delta(\cdot)$ is the Dirac δ-distribution), the two order parameters (14) and (16) coincide. According to (15), the instantaneous velocity of an oscillator at position θ, at time t, and with natural frequency ω is given by $v(\theta, t, \omega) = \omega + Kr(t)\sin(\psi(t) - \theta)$. The evolution of the probability density function is then governed by the continuity equation

$$\frac{\partial}{\partial t}\rho + \frac{\partial}{\partial \theta}(\rho v) = 0, \qquad (17)$$

subject to the conservation of the oscillators at time t and with frequency ω, that is, $\int_0^{2\pi} \rho(\theta, t, \omega)\, d\theta = 1$.[3]

Synchronization in the continuum-limit model: Similar to the finite-dimensional model (14),(15), the continuum-limit model (16),(17) displays a rich set of symmetries (Ott and Antonsen, 2008) and dynamics (Balmforth and Sassi, 2000; Martens et al., 2009). The saddle-node bifurcation from incoherence to synchrony in the finite-dimensional model (14),(15) (see Subsection 3.2) manifests itself in the infinite-dimensional model (16),(17) as a phase transition from the *uniform incoherent state* with density $\rho(\theta, t, \omega) = \frac{1}{2\pi}$ to the so-called *partially synchronized state*. The partially synchronized state is characterized by a subset of phase-locked oscillators rotating in unison whereas the remaining oscillators are incoherent. The synchronized set of oscillators are those satisfying $Kr > |\omega|$ such that $v(\theta, t, \omega) = 0$, and the incoherent ones are uniformly spread over the circle, see Figures 10(a) and 10(b) for a schematic illustration. This phase transition occurs when K exceeds some critical value K_{critical}. When K is further increased, more and more oscillators become entrained by the mean field (16) and join the set of phase-locked oscillators. For a frequency distribution $g(\omega)$ with bounded support, there exists a second critical parameter $K_{\mathrm{lock}} \geq K_{\mathrm{critical}}$, such that for $K > K_{\mathrm{lock}}$ all oscillators are phase-locked. This final stage of synchronization is illustrated in Figure 10(c). It is often referred to as the *fully phase-locked state*, and it is reminiscent of synchronization as displayed in the finite-dimensional model (14),(15).

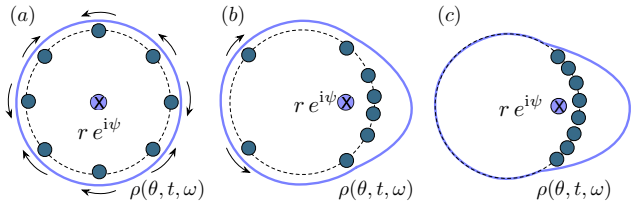

Fig. 10. Subfigure (a) displays the uniform incoherent state $\rho(\theta, t, \omega) = 1/(2\pi)$. Subfigure (b) illustrates the partially synchronized state, where a subset of oscillators rotates in unison and the remaining oscillators are incoherent. Subfigure (c) illustrates the fully phase-locked state.

Whereas the majority of the literature on the continuum-limit model (16),(17) focuses on the first phase transition and the calculation of K_{critical}, see (Kuramoto, 1984a; Crawford, 1994; Strogatz, 2000; Acebrón et al., 2005; Mirollo and Strogatz, 2007; Balmforth and Sassi, 2000; Ott and Antonsen, 2008; Chiba, 2010) and references therein, the articles (Ermentrout, 1985; van Hemmen and Wreszinski, 1993; Mirollo and Strogatz, 2005, 2007; Roberts, 2008; Verwoerd and Mason, 2011) discuss the fully phase-locked state and the calculation of K_{lock}. An extensive line of recent research in dynamics has been triggered by the work (Ott and Antonsen, 2008), which exploits the extensive symmetries of the continuum-limit model (16),(17) to construct simple solutions obeying low-dimensional ODE dynamics.

4 Basic Analysis Methods and Results

In this section, we review a few fundamental insights, we state some key lemmas, and we introduce some analysis methods which will be exploited throughout the rest of the paper.

4.1 Jacobian Analysis

We begin by drawing some insights from a Jacobian analysis. The right-hand side of (1) defines the vector field

[3] In some articles, the continuum-limit model (16)-(17) is presented with the density function $\tilde{\rho}(\theta, t, \omega) = \rho(\theta, t, \omega)g(\omega)$, which satisfies $\int_0^{2\pi} \tilde{\rho}(\theta, t, \omega) d\theta = g(\omega)$.

$f : \mathbb{T}^n \to \mathbb{R}^n$ with components

$$f_i(\theta) = \omega_i - \sum_{j=1}^{n} a_{ij} \sin(\theta_i - \theta_j)\,, \; i \in \{1, \dots, n\}\,. \quad (18)$$

Because $\frac{\partial}{\partial \theta_i} f_i(\theta) = -\sum_{j=1}^{n} a_{ij} \cos(\theta_i - \theta_j)$ and $\frac{\partial}{\partial \theta_j} f_i(\theta) = a_{ij} \cos(\theta_i - \theta_j)$, the Jacobian $J(\theta)$ of the coupled oscillator model (1) satisfies

$$J(\theta) = -B \operatorname{diag}(\{a_{ij} \cos(\theta_i - \theta_j)\}_{\{i,j\} \in \mathcal{E}}) B^T\,. \quad (19)$$

Thus, for phase cohesive angles $\theta \in \Delta_G(\pi/2)$, the Jacobian $J(\theta)$ equals minus the Laplacian matrix of the graph $G(\mathcal{V}, \mathcal{E}, \tilde{A})$ with strictly positive weights $\tilde{a}_{ij} = a_{ij} \cos(\theta_i - \theta_j) > 0$, for $\{i, j\} \in \mathcal{E}$. Hence, $J(\theta)$ is negative semidefinite, it inherits the sparsity of the graph $G(\mathcal{V}, \mathcal{E}, A)$, and its nullspace $\operatorname{Span}(\mathbf{1}_n)$ arises from the rotational symmetry of the vector field (18). These basic results are fundamental to various analysis approaches. To the best of the authors' knowledge this set of results was first established by Tavora and Smith (1972b,a), and it has since been rediscovered several times. Some consequences are collected in the following lemma, whose formal proof can be found in (Dörfler et al., 2013, Lemma 3).

Lemma 4.1 (Stable synchronization in $\Delta_G(\pi/2)$) *Consider the coupled oscillator model (1) with a connected graph $G(\mathcal{V}, \mathcal{E}, A)$ and frequencies $\omega \in \mathbf{1}_n^\perp$. If there exists an equilibrium $\theta^* \in \Delta_G(\pi/2)$, then*

(i) $-J(\theta^*)$ is a negative semidefinite Laplacian matrix;
(ii) the equilibrium manifold $[\theta^*] \in \Delta_G(\pi/2)$ is locally exponentially stable (modulo rotational symmetry); and
(iii) this equilibrium manifold is unique in $\bar{\Delta}_G(\pi/2)$ (modulo rotational symmetry).

The uniqueness statement *(iii)* follows from the more general fact that $f(\theta)$ is a one-to-one function (modulo rotational symmetry) for $\theta \in \bar{\Delta}_G(\pi/2)$, see the seminal work by Araposthatis et al. (1981, Corollary 1). Further consequences of the particular form of the Jacobian (19) in $\Delta_G(\pi/2)$ are collected below.

Frequency dynamics: The frequency dynamics obtained by differentiating the phase dynamics (1) are

$$\frac{d}{dt}\dot{\theta}_i = -\sum_{j=1}^{n} \tilde{a}_{ij}(t)(\dot{\theta}_i - \dot{\theta}_j)\,, \quad i \in \{1, \dots, n\}\,, \quad (20)$$

where $\tilde{a}_{ij}(t) = a_{ij} \cos(\theta_i(t) - \theta_j(t))$. The frequency dynamics (20) evolve on the tangent space of $\mathbb{T}^n$, that is, the Euclidean space $\mathbb{R}^n$. If the set $\bar{\Delta}_G(\gamma)$ is forward invariant and $\theta(0) \in \bar{\Delta}_G(\gamma)$ for some $\gamma \in [0, \pi/2[$, then $a_{ij}(t) \geq a_{ij} \cos(\gamma) > 0$, for $\{i, j\} \in \mathcal{E}$. Thus, the frequency dynamics (20) can be regarded as linear *consensus protocol* (3) with time-varying strictly-positive weights. Based on this observation, it can be shown that all frequencies $\dot{\theta}_i(t)$ synchronize exponentially, that is,

$$\|\dot{\theta}(t) - \omega_{\text{sync}} \mathbf{1}_n\|_2 \leq \|\dot{\theta}(0) - \omega_{\text{sync}} \mathbf{1}_n\|_2 e^{\lambda_{\text{fe}} t}\,, \quad (21)$$

where $\lambda_{\text{fe}} = -\lambda_2(L) \cos(\gamma)$. We refer to (Chopra and Spong, 2009, Theorem 3.1) and (Dörfler and Bullo, 2012b, Theorem 4.1) for a formal proof, and to (Schmidt et al., 2012, Lemma 3.5) and (Dörfler and Bullo, 2012b, Theorem 4.1) for extensions to general coupling functions and time-delays.

Contraction and incremental stability: Assume again that $\bar{\Delta}_G(\gamma)$ is forward invariant for some $\gamma \in [0, \pi/2[$. Since $J(\theta)$ is negative semidefinite in $\bar{\Delta}_G(\gamma)$, it follows that the coupled oscillator dynamics (1) are *contracting*[4] relative to the nullspace $\mathbf{1}_n$. Consequently, the dynamics (1) are incrementally exponentially stable (modulo symmetry), that is, given any two initial values $\theta(0), \tilde{\theta}(0) \in \bar{\Delta}_G(\gamma)$, there is a pseudo-metric $d : \mathbb{T}^n \times \mathbb{T}^n \to \mathbb{R}_{\geq 0}$ (more precisely, a metric modulo symmetry)[5] and constants $c_1 \geq 1$ and $c_2 > 0$ such that

$$d\big(\theta(t), \tilde{\theta}(t)\big) \leq c_1 e^{-c_2 t} d\big(\theta(0), \tilde{\theta}(0)\big), \quad \forall\, t \geq 0\,. \quad (22)$$

The application of contraction analysis to the coupled oscillator model (1) yields the incremental exponential stability (22) in ℓ_2-type metrics (Chung and Slotine, 2010, Theorem 7) or in ℓ_∞-type metrics (Forni and Sepulchre, 2012, Example 6). Choi et al. (2011a, Theorem 4.1) report the incremental stability (22) in an ℓ_1-metric. Finally, for discontinuous and monotone coupling functions and complete interaction graphs the total variation distance provides yet another ℓ_1-type contraction metric (Mauroy and Sepulchre, 2012).

Jacobian analysis beyond $\Delta_G(\pi/2)$: The results discussed so far in Subsection 4.1 are applicable only to angles inside the phase cohesive set $\Delta_G(\pi/2)$, where all weights $\tilde{a}_{ij} = a_{ij} \cos(\theta_i - \theta_j)$ are strictly positive for $\{i, j\} \in \mathcal{E}$ and the Laplacian properties of the Jacobian $J(\theta)$ can be exploited. Outside the set $\Delta_G(\pi/2)$, the associated state-dependent graph $G(\mathcal{V}, \mathcal{E}, \tilde{A})$ may at times be disconnected and/or have negative weights $\tilde{a}_{ij} = a_{ij} \cos(\theta_i - \theta_j) < 0$. In this more general setting, the standard methods from algebraic and spectral

[4] We refer the reader to (Lohmiller and Slotine, 1998; Sontag, 2010) for a treatment of contraction analysis and to (Wang and Slotine, 2005; Russo et al., 2010; Forni and Sepulchre, 2012) for its extension to systems with symmetries.

[5] The pseudo-metric d is a nonnegative and symmetric function $(d(\theta_1, \theta_2) = d(\theta_2, \theta_1))$ satisfying the triangle inequality $d(\theta_1, \theta_2) \leq d(\theta_1, \theta_3) + d(\theta_3, \theta_2)$ and $d(\theta_1, \theta_1) = 0$ if and only if $[\theta_1] = [\theta_2]$. The pseudo-metric d is a proper distance function on the quotient manifold $\mathbb{T}^n/\mathbb{S}^1$.

graph theory cannot be applied and many puzzling examples are known (Araposthatis et al., 1981). A necessary condition for stability of arbitrary equilibrium manifolds $[\theta^*] \subset \mathbb{T}^n$ is that the graph induced by the Jacobian $J(\theta^*)$ possess a spanning tree with strictly positive weights $\tilde{a}_{ij} > 0$ along its edges (Do et al., 2012). Sufficient stability and instability conditions can be derived if the graph induced by $J(\theta^*)$ admits certain cutsets (Araposthatis et al., 1981; Bergen and Hill, 1981; Chandrashekhar and Hill, 1986; Mallada and Tang, 2010). Finally, for the complete graph with uniform weights (see the Kuramoto model (2)), additional insights and identities related to the Jacobian (19) can be found in (Aeyels and Rogge, 2004; Mirollo and Strogatz, 2005; Verwoerd and Mason, 2008; Bronski et al., 2012).

4.2 Potential Landscape Analysis

The potential energy $U : \mathbb{T}^n \to \mathbb{R}$ of the spring network in Figure 1 is, up to an additive constant,

$$U(\theta) = \sum\nolimits_{\{i,j\}\in\mathcal{E}} a_{ij}\big(1 - \cos(\theta_i - \theta_j)\big)\,. \tag{23}$$

For the complete graph with uniform weights K/n, the magnitude r of the order parameter and the potential energy $U(\theta)$ are related by $\frac{2}{n}U(\theta) = 1 - r^2$. One can easily verify that the phase-synchronized state is a local minimum of the potential energy.

Given the potential energy in equation (23), the coupled oscillator model (1) can be reformulated as the forced gradient system

$$\dot{\theta}_i = \omega_i - \frac{\partial}{\partial\theta_i}U(\theta)\,, \qquad i \in \{1,\dots,n\}\,. \tag{24}$$

This rewriting clarifies the competition between the synchronization-enforcing coupling through $U(\theta)$ and the synchronization-inhibiting heterogeneous natural frequencies ω_i. The unforced system (24) with $\omega = \mathbf{0}_n$ is a negative gradient flow $\dot{\theta} = -\partial U(\theta)/\partial\theta$ with U as natural Lyapunov function.

Since the Jacobian $J(\theta)$ is the negative Hessian of the potential $U(\theta)$, Lemma 4.1 implies that any equilibrium in $\Delta_G(\pi/2)$ is a local minimizer of $U(\theta)$. Of particular interest are so-called $\mathbb{S}^1$-*synchronizing graphs* for which all critical points of (23) are hyperbolic, the phase-synchronized state is the global minimum of $U(\theta)$, and all other critical points are local maxima or saddle points. The class of $\mathbb{S}^1$-synchronizing graphs includes, among others, complete graphs and acyclic graphs (Monzón and Paganini, 2005; Canale and Monzón, 2008; Sarlette, 2009; Canale et al., 2010b,a). These basic results motivated the study of the critical points and of the curvature of the potential energy $U(\theta)$ in the literature on the theory and applications of synchronization, including, for example, the study of transient stability in power systems and the design of motion coordination controllers for planar vehicles, see Subsections 2.1 and 2.2. Some direct consequences of the gradient formulation (24) and of the associated Hessian matrix (19) will be presented in Section 5.

4.3 Absolute and Incremental Boundedness

In this subsection we start from the basic observation that the sinusoidal interaction terms in equation (1) are upper bounded by the nodal degree $\deg_i = \sum_{j=1}^n a_{ij}$ of each oscillator. Hence, the natural frequencies ω have to satisfy certain bounds, relative to the nodal degree, if synchronized solution is to exist.

Lemma 4.2 (Necessary sync condition) *Consider the coupled oscillator model* (1) *with graph* $G(\mathcal{V},\mathcal{E},A)$, *frequencies* $\omega \in \mathbf{1}_n^\perp$, *and nodal degree* $\deg_i = \sum_{j=1}^n a_{ij}$ *for* $i \in \{1,\dots,n\}$. *If there exists a synchronized solution* $\theta \in \bar{\Delta}_G(\gamma)$ *for some* $\gamma \in [0,\pi/2]$, *then the following conditions hold:*

1) **Absolute bound:** *For each node* $i \in \{1,\dots,n\}$,

$$\deg_i \sin(\gamma) \geq |\omega_i|\,; \tag{25}$$

2) **Incremental bound:** *For distinct* $i,j \in \{1,\dots,n\}$,

$$(\deg_i + \deg_j)\sin(\gamma) \geq |\omega_i - \omega_j|\,. \tag{26}$$

This lemma follows directly from the fact that synchronized solutions must satisfy $\dot{\theta}_i = 0$ and $\dot{\theta}_i - \dot{\theta}_j = 0$ for all $i,j \in \{1,\dots,n\}$, see (Dörfler et al., 2013, Lemma 3) for a formal proof. The necessary conditions (25) and (26) are conservative estimates since they can be attained only if all angular distances $|\theta_i - \theta_k|$ and $|\theta_j - \theta_k|$ take the value γ, which is generally not possible. We will show in Lemma 6.4 below how to improve these necessary conditions for the complete graph.

5 Synchronization of Identical Oscillators

In this section we present several analysis approaches and results for the study of synchronization in coupled homogeneous oscillators, that is, oscillators models of the form (1) with identical natural frequencies.

5.1 Phase Synchronization

It can be easily verified that for non-zero and dissimilar natural frequencies $\omega \in \mathbf{1}_n^\perp$, the coupled oscillator model (1) does not admit a phase-synchronized solution of the form $\theta_i(t) = \theta_j(t)$ for all $i,j \in \{1,\dots,n\}$. On the contrary, if all natural frequencies are identical, $\omega_i \equiv \omega_0$ for

all $i \in \{1, \dots, n\}$, then a transformation of the oscillator network (1) to a rotating frame with frequency ω_0 yields

$$\dot{\theta}_i = -\sum_{j=1}^{n} a_{ij} \sin(\theta_i - \theta_j), \qquad i \in \{1, \dots, n\}. \quad (27)$$

An elegant analysis of the coupled oscillator model (27) follows the insights developed in Subsections 4.1 and 4.2. System (27) is a negative gradient flow $\dot{\theta} = -\partial U(\theta)/\partial\theta$ defined by the smooth function $U(\theta)$ with compact sublevel sets. Hence, the LaSalle Invariance Principle (Khalil, 2002, Theorem 4.4) asserts that every solution converges to set of critical points $\{\theta \in \mathbb{T}^n \mid \partial U(\theta)/\partial\theta = \mathbf{0}_n\}$. By Lemma 4.1, the phase-synchronized equilibrium manifold $[\theta] \in \bar{\Delta}_G(0)$ is locally exponentially stable. Moreover, for a $\mathbb{S}^1$-synchronizing graph, all other equilibria are unstable. We arrive at the following result presented in (Jadbabaie et al., 2004; Monzón and Paganini, 2005; Scardovi et al., 2007; Sepulchre et al., 2007).

Theorem 5.1 (Phase synchronization) *Consider the coupled oscillator model* (1) *with a connected graph* $G(\mathcal{V}, \mathcal{E}, A)$ *and with natural frequencies* $\omega \in \mathbb{R}^n$. *The following statements are equivalent:*

(i) **Homogeneity:** *there exists a constant* $\omega_0 \in \mathbb{R}$ *such that* $\omega_i = \omega_0$ *for all* $i \in \{1, \dots, n\}$; *and*
(ii) **Local phase sync:** *there exists a locally exponentially stable phase synchronization manifold* $\bar{\Delta}_G(0)$.

If the two equivalent cases (i) and (ii) are true, the following statements hold:

1) **Global convergence:** *For all initial angles* $\theta(0) \in \mathbb{T}^n$, *the frequencies* $\dot{\theta}(t)$ *converge to* $\omega_0 \mathbf{1}_n$ *and the phases* $\theta(t)$ *converge to* $\{\theta \in \mathbb{T}^n \mid \partial U(\theta)/\partial\theta = \mathbf{0}_n\}$; *and*
2) **Almost global stability:** *If* $G(\mathcal{V}, \mathcal{E}, A)$ *is* $\mathbb{S}^1$*-synchronizing, the region of attraction of the phase synchronization manifold* $\bar{\Delta}_G(0)$ *is almost all of* $\mathbb{T}^n$.

A representative simulation is shown in Figure 12(a) below. The corresponding discrete-time analog to Theorem 5.1 can be found in (Klein, 2008; Klein et al., 2008; Scardovi et al., 2007). If higher order models with dynamic coupling are considered, then almost globally stable phase synchronization can be achieved for arbitrary connected (and also directed) graphs (Scardovi et al., 2007; Sepulchre et al., 2008; Lunze, 2011).

5.2 Consensus, Contraction, & Convexity

The interest of the control community in oscillator networks (1) was initially sparked by Jadbabaie et al. (2004) and Moreau (2005), who analyzed networks of identical oscillators as nonlinear extensions of the consensus protocol (3). Indeed, for zero natural frequencies $\omega = \mathbf{0}_n$ and for angles contained in an open semicircle $\theta \in \mathrm{Arc}_n(\pi)$, the dynamics (27) can be projected onto the real line via the local coordinate map $\varphi :]-\pi/2, \pi/2[^n \to \mathbb{R}^n$ defined by $x_i = \varphi_i(\theta_i) = \tan(\theta_i)$. With this projection proposed by Moreau (2005), the dynamics (27) are rewritten as the consensus-type model

$$\dot{x}_i = -\sum_{j=1}^{n} b_{ij}(x)(x_i - x_j), \quad (28)$$

where $b_{ij}(x) = a_{ij}\sqrt{(1+x_i^2)/(1+x_j^2)} \geq 0$. In particular, for $\theta \in \overline{\mathrm{Arc}}_n(\gamma)$ for some $\gamma \in [0, \pi[$, we have that $b_{ij}(x) \geq a_{ij}/\sec(\gamma/2) > 0$ is strictly positive for $\{i, j\} \in \mathcal{E}$. A similar viewpoint is taken by Jadbabaie et al. (2004), where the coupled oscillator model (27) is equivalently written as

$$\dot{\theta}_i = -\sum_{j=1}^{n} c_{ij}(\theta)(\theta_i - \theta_j), \quad (29)$$

where $c_{ij}(\theta) = a_{ij}\,\mathrm{sinc}(\theta_i - \theta_j) \geq 0$. Again, we have that $c_{ij}(\theta) \geq a_{ij}\,\mathrm{sinc}(\gamma) > 0$ for $\{i, j\} \in \mathcal{E}$ and $\theta \in \overline{\mathrm{Arc}}_n(\gamma)$, $\gamma \in [0, \pi[$. Further consensus-theoretical derivations of the oscillator network (27) can be found in (Olfati-Saber, 2006; Sarlette and Sepulchre, 2009; Sepulchre, 2011).

In both formulations (28) and (29), the dynamics (27) are regarded as a consensus protocol (3) with strictly positive weights whose values are time-varying or state-dependent. This interpretation is well defined provided that $\theta(t) \in \overline{\mathrm{Arc}}_n(\gamma)$ for all $t \geq 0$ and for some $\gamma \in [0, \pi[$. Different Lyapunov functions can be used to assure this boundedness, e.g., the potential function $U(\theta)$ or standard quadratic Lyapunov functions used in consensus theory. Generally, the level sets of these Lyapunov functions are hard to characterize and provide poor estimates on the region of attraction. Another natural Lyapunov function is simply the length of the shortest arc containing all oscillators. This approach relies upon the *contraction property*, it has been developed for general nonlinear consensus systems, and it aims at showing that the convex hull of all states is decreasing, see (Moreau, 2004, 2005; Lin et al., 2007; Sepulchre, 2011) and the review by Sepulchre et al. (2010, Section 2).

Recall the geodesic distance on $\mathbb{S}^1$ and define the continuous function $V : \mathbb{T}^n \to [0, \pi]$ by

$$V(\psi) = \max\{|\psi_i - \psi_j| \mid i, j \in \{1, \dots, n\}\}. \quad (30)$$

If all angles at time t are contained in an arc of length strictly less than π, then the arc length $V(\theta(t)) = \max_{i,j \in \{1,\dots,n\}} |\theta_i(t) - \theta_j(t)|$ is a Lyapunov function candidate for phase synchronization, see Figure 11. Intuitively, the oscillators $\theta_\ell(t)$ and $\theta_r(t)$ at both boundaries are pulled towards their neighbors in the interior $\mathrm{Arc}_n(V(\theta(t)))$, and the Lyapunov function $V(\theta(t))$ is non-increasing. The technical analysis is slightly more

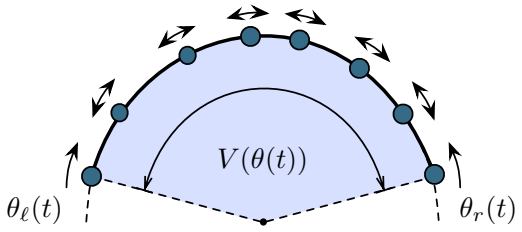

Fig. 11. Illustration of the Lyapunov function candidate $V(\theta(t))$ for angles in an open semicircle $\theta(t) \in \mathrm{Arc}_n(\pi)$. The oscillators at the boundaries of the arc containing all oscillators $\overline{\mathrm{Arc}}_n(V(\theta(t)))$ are denoted by $\theta_\ell(t)$ and $\theta_r(t)$.

subtle since the function $V(\theta(t))$ is continuous but not necessarily differentiable when the maximum geodesic distance is attained by more than one pair of oscillators. In summary, we state the following result, which follows from the analysis of nonlinear consensus protocols, see (Lin et al., 2007, Theorem 3.6 and 3.7) and (Moreau, 2005, Theorems 1 and 2) for continuous and discrete-time results.

Theorem 5.2 (Contraction in Open Semicircle $\mathrm{Arc}_n(\pi)$) *Consider the coupled oscillator model* (27) *with a connected graph $G(\mathcal{V}, \mathcal{E}, A)$ and $\omega = \mathbf{0}_n$. Each set $\overline{\mathrm{Arc}}_n(\gamma)$, for $\gamma \in [0, \pi[$, is positively invariant, and each trajectory originating in $\overline{\mathrm{Arc}}_n(\gamma)$ achieves exponential phase synchronization, that is,*

$$\|\theta(t) - \theta_{\mathrm{avg}}\mathbf{1}_n\|_2 \leq \|\theta(0) - \theta_{\mathrm{avg}}\mathbf{1}_n\|_2 e^{\lambda_{\mathrm{ps}} t}\,, \qquad (31)$$

where $\lambda_{\mathrm{ps}} = -\lambda_2(L)\,\mathrm{sinc}(\gamma)$ and $\theta_{\mathrm{avg}} = \sum_{i=1}^n \theta_i(0)/n$ is the average initial phase. [6]

Theorem 5.2 also holds for directed and time-variant graphs, it applies to more general interaction functions, and it can be extended to time-delayed systems. Applications to oscillator networks and extensions can be found in (Lin et al., 2007; Moreau, 2005; Münz et al., 2009; Ha et al., 2010a; Sarlette, 2009; Ha et al., 2010a; Dörfler and Bullo, 2011, 2012b; Schmidt et al., 2012). We will revisit this literature in Section 6.

Remark 2 (A control-theoretical perspective on synchronization) *As established in Theorems 5.1 and 5.2, the phase-synchronized set $\bar{\Delta}_G(0) = \overline{\mathrm{Arc}}_n(0)$ is locally exponentially stable provided all natural frequencies are identical. While phase synchronization is not possible for dissimilar natural frequencies, a certain degree of phase cohesiveness can still be achieved. Indeed, the coupled oscillator model* (1) *can be regarded as an exponentially stable system subject to the disturbance $\omega \in \mathbf{1}_n^\perp$ and synchronization can be studied using classic control-theoretical concepts such as input-to-state stability, practical stability, ultimate boundedness (Khalil, 2002) or their incremental versions (Angeli, 2002). In control-theoretical terminology, phase cohesiveness can then be described as "practical phase synchronization." Compared to prototypical nonlinear control examples, various additional challenges arise in the analysis of the coupled oscillator model* (1) *due to the bounded and non-monotone sinusoidal coupling, the compact state space, and the existence of multiple equilibria.* □

[6] This "average" of angles (points on $\mathbb{S}^1$) is well-defined in an open semi-circle. If the parametrization of θ has no discontinuity inside the arc containing all angles, then the average can be obtained by the usual formula.

5.3 Phase Balancing and Pattern Formation

As compared with phase synchronization, only few results are known about phase balancing. This asymmetry may be caused by the fact that phase synchrony is studied in more applications than phase balancing. Moreover, the phase-synchronized set $\overline{\mathrm{Arc}}_n(0)$ admits a very simple geometric characterization, whereas the phase-balanced set Bal_n has a complicated structure consisting of multiple disjoint subsets. The number of these subsets grows combinatorially with the number of nodes n.

Consider the coupled oscillator model (27). By inverting the direction of time, we obtain

$$\dot{\theta}_i = \sum\nolimits_{j=1}^n a_{ij} \sin(\theta_i - \theta_j)\,, \qquad i \in \{1, \dots, n\}\,. \qquad (32)$$

In what follows, an undirected graph $G(\mathcal{V}, \mathcal{E}, A)$ is *circulant* if the adjacency matrix $A = A^T$ is a circulant matrix. Circulant graphs are highly symmetric graphs; examples include complete graphs, complete bipartite graphs, and ring graphs. [7] For circulant and uniformly weighted graphs, the coupled oscillator model (32) achieves phase balancing. The following theorem summarizes several results originally presented in (Sepulchre et al., 2007, Theorem 1) and (Sepulchre et al., 2008, Theorem 2).

Theorem 5.3 (Phase balancing) *Consider the coupled oscillator model* (32) *with a connected, undirected, uniformly weighted, and circulant graph $G(\mathcal{V}, \mathcal{E}, A)$. The following statements hold:*

1) **Local phase balancing:** *The phase-balanced set Bal_n is locally asymptotically stable; and*
2) **Almost global stability:** *If the graph $G(\mathcal{V}, \mathcal{E}, A)$ is complete, then the region of attraction of the stable phase-balanced set Bal_n is almost all of $\mathbb{T}^n$.*

The proof of Theorem 5.3 is similar to that of Theorem 5.1: convergence is established by a potential function

[7] A gallery and examples of circulant graphs can be found at `http://mathworld.wolfram.com/CirculantGraph.html`.

argument and the local (in)stability of equilibria is established by a Jacobian argument. An illustrative simulation is shown in Figure 12(b) below. For general connected graphs, the conclusions of Theorem 5.3 are not true. As a remedy to achieve almost globally stable phase balancing, higher order models with dynamic coupling can be considered, see (Scardovi et al., 2007; Sepulchre et al., 2008).

Alternatively, phase balancing can also be achieved by coupling functions with higher-order harmonics. For example, a modification of model (32) is

$$\dot{\theta}_i = \sum_{j=1}^{n} \sum_{\ell=1}^{m} \frac{K_\ell \cdot a_{ij}}{\ell} \sin\big(\ell(\theta_i - \theta_j)\big)\,, \qquad (33)$$

where $K_\ell \in \mathbb{R}$ are appropriate gains, and $m \in \mathbb{N}$ divides n. The dynamics (33) are again a gradient system whose critical points include symmetric balanced (m,n)-patterns; recall Figure 9 for a schematic illustration. The following result is given in (Sepulchre et al., 2007, Theorem 7) and (Sepulchre et al., 2008, Theorem 7).

Theorem 5.4 (Pattern formation) *Consider the coupled oscillator model* (33) *with a connected, undirected, uniformly weighted, and circulant graph* $G(\mathcal{V},\mathcal{E},A)$. *Let* $m \in \mathbb{N}$ *be a divisor of* n, *let* $K_\ell > 0$ *for* $\ell \in \{1,\dots,m-1\}$, *and let* $K_m < 0$ *be sufficiently small. Then each symmetric balanced* (m,n)*-pattern is a locally exponentially stable equilibrium manifold.*

Two representative simulations are shown in Figures 12(c) and 12(d). Theorem 5.4 can also be extended to non-circulant (and directed) graphs through dynamic coupling, see (Sepulchre et al., 2008, Theorem 8). Notice that Theorem 5.4 establishes only the local stability of (m,n) patterns; the dynamics (33) feature other stable equilibria.

6 Synchronization in Complete Networks

In this section, we study heterogeneous oscillators coupled in a complete graph with uniform weights $a_{ij} = K/n$. In this case, the coupled oscillator model (1) reduces to the celebrated Kuramoto model given in (2). The Kuramoto model will reach synchronization provided that the coupling gain K is larger than a critical value K_{critical}, which depends on the dissimilarity among the natural frequencies ω. Starting from Winfree's and Kuramoto's pioneering work (Winfree, 1967; Kuramoto, 1975, 1984a), this trade-off has been characterized by parametric inequalities. In what follows, we review various estimates of the critical coupling strength K_{critical} to characterize the on-set of synchronization as well as the ultimate stage of synchronization. We consider both infinite-dimensional as well as finite-dimensional Kuramoto models.

6.1 Infinite-Dimensional Kuramoto Models

In his ingenious analysis of the continuum-limit model (16)-(17) Kuramoto considered continuous, even, and unimodal distributions $g(\omega)$ of the natural frequencies (achieving their maximum at $g(0)$), and found that phase-locked solutions (if existent) must satisfy the *self-consistency equation* (Kuramoto, 1984a, Eq. (5.4.26))

$$r = Kr \int_{-\pi/2}^{\pi/2} \cos^2(\theta) g(Kr\sin(\theta))\, d\theta\,. \qquad (34)$$

One trivial solution to the self-consistency equation (34) is $r = 0$ corresponding to the uniform incoherent state shown in Figure 10(a). The second solution for $r > 0$ corresponds to the partially synchronized state illustrated in Figure 10(b). When canceling the variable r from both sides of (34) and taking the limit $r \searrow 0$, the self-consistency equation (34) delivers the bifurcation parameter

$$K_{\text{critical}} = \frac{2}{\pi g(0)}\,. \qquad (35)$$

Kuramoto conjectured that the uniform incoherent state would become unstable for $K > K_{\text{critical}}$ and concluded famously that "surprisingly enough, this seemingly obvious fact seems difficult to prove." The resolution of this long-standing conjecture and Kuramoto's ingenious yet incomplete analysis inspired generations of scientists, see (Strogatz, 2000) for an historical account. We present the following general result taken from the recent (Chiba, 2010, Theorem 3.5).

Theorem 6.1 (Instability of the incoherent state) *Consider the infinite-dimensional Kuramoto model* (16),(17) *with coupling gain* K *and frequency distribution* $g : \mathbb{R} \to \mathbb{R}_{\geq 0}$. *Let* $\{y_1, y_2, \dots\}$ *be the roots of the equation*

$$\lim_{x \searrow 0} \int_{-\infty}^{\infty} \frac{\omega - y}{x^2 + (w-y)^2}\, g(\omega)\, d\omega = 0\,, \qquad (36)$$

and assume $g(\omega)$ *is continuous at* $\{y_1, y_2, \dots\}$. *If*

$$K > K_{\text{critical}} = \frac{2}{\pi \sup_j g(y_j)}\,,$$

then the incoherent state $\rho(\theta,t,\omega) = 1/(2\pi)$ *is unstable.*

Notice that Theorem 6.1 is fairly general and includes bimodal distributions. It can be shown that for a continuous, even, and unimodal distribution $g(\omega)$, the unique root of (36) is given by $y_1 = 0$, see (Chiba, 2010, Corollary 3.6). This observation leads to the following corollary, which can be found in (Crawford, 1994; Balmforth and Sassi, 2000; Acebrón et al., 2005; Mirollo and Strogatz, 2007; Ott and Antonsen, 2008; Martens et al., 2009; Chiba, 2010), and references therein.

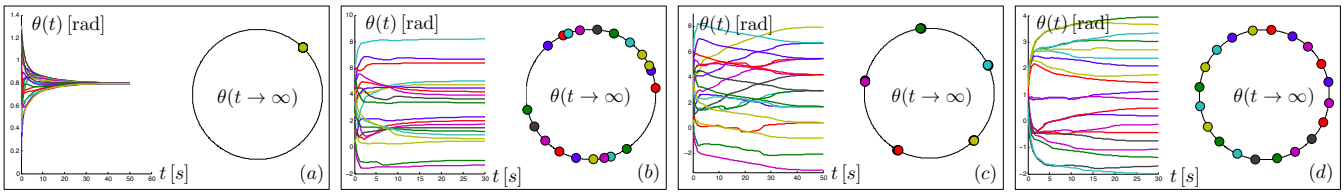

Fig. 12. Synchronization in a network of identical oscillators with $n = 20$, $\omega = \mathbf{0}_n$, and a ring graph $G(\mathcal{V}, \mathcal{E}, A)$ with unit weights. Subfigure (a) shows phase synchronization achieved by the oscillator network (27). Subfigure (b) shows phase balancing achieved by the oscillator network (32). Subfigure (c) and (d) show pattern formation achieved by the oscillator network (33) for the symmetric balanced $(5, 20)$-pattern and $(20, 20)$-pattern corresponding to the splay state.

Corollary 6.2 (Instability beyond Kuramoto's critical transition point) *Consider the infinite-dimensional Kuramoto model* (16),(17) *with coupling gain* K *and frequency distribution* $g : \mathbb{R} \to \mathbb{R}_{\geq 0}$. *Suppose that* $g(\omega)$ *is continuous at the origin, even, and unimodal. If* K *is greater than* K_{critical} *as given in* (35), *then the incoherent state* $\rho(\theta, t, \omega) = 1/(2\pi)$ *is unstable.*

A linear stability analysis of the associated partially-synchronized state illustrated in Figure 10(b) is discussed by Mirollo and Strogatz (2007) and reveals linear neutral stability. To the best of the authors' knowledge, a nonlinear stability analysis of the partially-synchronized state is still outstanding.

If the distribution $g(\omega)$ is restricted to have bounded support, then the fully phase-locked state (illustrated in Figure 10(c)) can be achieved when the coupling K is larger than the second critical threshold $K_{\text{lock}} \geq K_{\text{critical}}$. In this case, two distributions of interest are the uniform distribution and the bipolar distribution given by

$$g_{\text{unif}} : [-\omega_0, +\omega_0] \to \mathbb{R}\,, \quad g_{\text{unif}}(\omega) = \frac{1}{2\omega_0},$$
$$g_{\text{bip}} : [\omega_{\min}, \omega_{\max}] \to \mathbb{R}\,,$$
$$g_{\text{bip}}(\omega) = p \cdot \delta(\omega - \omega_{\max}) + (1-p) \cdot \delta(\omega - \omega_{\min}),$$

where $\omega_0 > 0$, $\omega_{\max} > \omega_{\min}$, and $p \in [0, 1]$. These two distributions are particularly interesting since they yield the smallest and the largest threshold K_{lock}.

Theorem 6.3 (Full phase locking thresholds) *Consider the infinite-dimensional Kuramoto model* (16),(17) *with coupling gain* K *and frequency distribution* $g : \mathbb{R} \to \mathbb{R}_{\geq 0}$ *with bounded support. The following statements hold for the full phase-locking threshold* K_{lock}*:*

(i) **Lower bound:** *For any continuous, even, and unimodal* $g : [-\omega_0, +\omega_0] \to \mathbb{R}$, *where* $\omega_0 > 0$, *we have* $K_{\text{lock}} \geq 4\,\omega_0/\pi$. *Moreover, for the uniform distribution* $g_{\text{unif}}(\omega)$, *we have* $K_{\text{lock}} = 4\,\omega_0/\pi$.

(ii) **Upper bound:** *For any* $g : [\omega_{\min}, \omega_{\max}] \to \mathbb{R}_{\geq 0}$, *where* $\omega_{\max} > \omega_{\min}$, *we have* $K_{\text{lock}} \leq \omega_{\max} - \omega_{\min}$. *Moreover, for the bipolar distribution* $g_{\text{bip}}(\omega)$ *we have* $K_{\text{lock}} = \omega_{\max} - \omega_{\min}$.

A proof of the lower bound (i) can be found in (Ermentrout, 1985, Corollary 2(b)) and (Mirollo and Strogatz, 2007). Notice that the two thresholds K_{critical} (reported in (35)) and K_{lock} coincide for the uniform distribution:

$$K_{\text{lock}} = \frac{2}{\pi g_{\text{unif}}(0)} = K_{\text{critical}}\,.$$

This remarkable identity was also observed by van Hemmen and Wreszinski (1993); Mirollo and Strogatz (2007); Roberts (2008); Verwoerd and Mason (2011). The upper bound (ii) on bipolar distributions has been proved by van Hemmen and Wreszinski (1993) and earlier by Ermentrout (1985) for the symmetric case ($p = 1/2$ and $\omega_{\max} = -\omega_{\min} = \omega_0$). Bipolar and more general bimodal frequency distributions $g(\omega)$ have attracted tremendous research interest by dynamicists thanks to their rich bifurcation diagram, see (Acebrón et al., 2005; Martens et al., 2009). The uniform and bipolar distributions are shown in Figure 13 together with the associated stationary phase distributions in the critical case $K \searrow K_{\text{lock}}$ (explicitly calculated by van Hemmen and Wreszinski (1993)). For later reference, Figure 13 also shows the tripolar distribution $g_{\text{trip},n}(\omega) = \frac{1}{n}\delta(\omega - \omega_0) + \frac{n-2}{n}\delta(\omega_0) + \frac{1}{n}\delta(\omega + \omega_0)$ and its associated phase distribution (calculated by Chopra and Spong (2009, Proof of Theorem 2.1)) for $n \to \infty$.

6.2 Finite-Dimensional Kuramoto Models

In the finite-dimensional case, various necessary, sufficient, implicit, and explicit estimates of the critical coupling strength K_{critical} have been proposed (van Hemmen and Wreszinski, 1993; Aeyels and Rogge, 2004; Jadbabaie et al., 2004; Acebrón et al., 2005; Mirollo and Strogatz, 2005; De Smet and Aeyels, 2007; Chopra and Spong, 2009; Verwoerd and Mason, 2008, 2009; Chung and Slotine, 2010; Ha et al., 2010a; Ha and Slemrod, 2011; Choi et al., 2011a; Franci et al., 2011; Dörfler and Bullo, 2011, 2012b; Schmidt et al., 2012). We refer to (Dörfler and Bullo, 2011) for a comprehensive historical overview and present only the best known results here.

Necessary, explicit, and tight conditions: The necessary condition (26) evaluated for $\gamma \nearrow \pi/2$ gives the

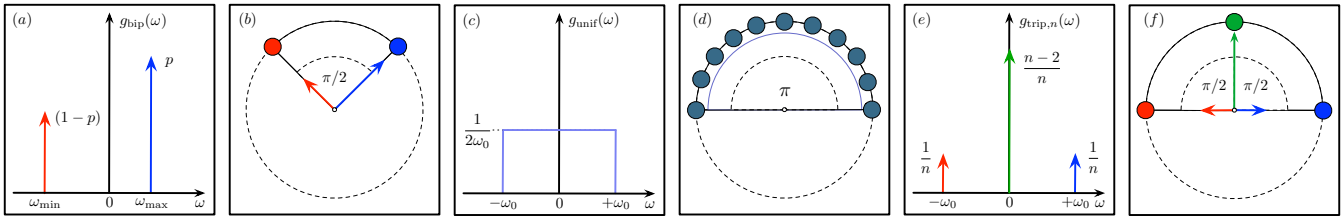

Fig. 13. Extremal distributions $g(\omega)$ of the natural frequencies and their stationary phase distributions in the critical case $K \searrow K_{\mathrm{lock}}$: Panels (a) and (b) show the non-symmetric bipolar distribution $g_{\mathrm{bip}}(\omega) = p \cdot \delta(\omega - \omega_{\max}) + (1-p) \cdot \delta(\omega - \omega_{\min})$ and its associated bipolar phase distribution. Panels (c) and (d) show the uniform $g_{\mathrm{unif}}(\omega) = 1/(2\omega_0)$ and its associated uniform phase distribution. Finally, panels (e) and (f) show the tripolar distribution $g_{\mathrm{trip},n}(\omega) = \frac{1}{n}\delta(\omega - \omega_0) + \frac{n-2}{n}\delta(\omega_0) + \frac{1}{n}\delta(\omega + \omega_0)$ and its associated tripolar phase distribution for $n \to \infty$.

following lower bound for the critical coupling:

$$K \geq K_{\mathrm{critical}} \triangleq \frac{n \cdot (\omega_{\max} - \omega_{\min})}{2(n-1)} \,. \tag{37}$$

Of course, this often-reported lower bound (37) is generally conservative. The following tighter lower bound has been constructed by Chopra and Spong (2009).

Lemma 6.4 (Explicit, necessary, and tight critical coupling) *Consider the Kuramoto model* (2) *with* $n \geq 2$ *oscillators, natural frequencies* $\omega \in \mathbf{1}_n^\perp$, *and coupling strength* K. *Define* $\gamma \in [\pi/2, \pi]$ *by*

$$\gamma = 2 \arcos\left(\frac{-(n-2) + \sqrt{(n-2)^2 + 32}}{8} \right) . \tag{38}$$

The Kuramoto model has a frequency-synchronized solution only if the coupling strength K *is larger than a critical value, that is,*

$$K \geq K_{\mathrm{critical}} \triangleq \frac{n \cdot (\omega_{\max} - \omega_{\min})}{2\left(\sin(\gamma) + (n-2)\sin(\gamma/2)\right)} \,. \tag{39}$$

Moreover, condition (39) *is tight: for* $\omega = \omega_{\mathrm{trip}} \triangleq \omega_0 \cdot (+1, -1, \mathbf{0}_{n-1})$ *with* $\omega_0 \in \mathbb{R}$ *and for any of its permutations, there exists a synchronous solution if and only if* $K \geq K_{\mathrm{critical}}$.

Notice that the bound (39) equals the bound (37) for $n = 2$ and for $n \to \infty$, and is a strict improvement otherwise. The bound (39) is reported in (Chopra and Spong, 2009, Eqs. (8) and (11)) and is computed using optimization techniques. Though not explicitly stated by Chopra and Spong (2009), it can be verified from their proof that the lower bound (38)-(39) is tight for $\omega = \omega_{\mathrm{trip}}$. In the critical case $K = K_{\mathrm{critical}}$, the associated arc-invariant equilibrium manifold is given by $[\theta^*] = [(+\gamma/2, -\gamma/2, \mathbf{0}_{n-2})]$. In the limit $n \to \infty$ this choice of natural frequencies ω corresponds to the tripolar distribution in Figure 13(e), and the associated phases $[\theta^*]$ are shown in Figure 13(f).

Exact and implicit conditions: The articles (Aeyels and Rogge, 2004; Mirollo and Strogatz, 2005; Verwoerd and Mason, 2008) derive a set of implicit consistency equations for the *exact* critical coupling strength K_{critical} for which frequency-synchronized solutions exist. The consistency equation can be easily motivated. Each equilibrium solution to the Kuramoto model (14),(15) is characterized by $[\theta^*] \in \mathbb{T}^n$ such that the left-hand side of (15) equals zero. We denote the corresponding value of the order parameter (14) by $r_\infty \in [0, 1]$ and, without loss of generality, we assume that its phase ψ is zero. Hence, we arrive at the equations

$$\begin{aligned} \omega_i &= K r_\infty \sin(\theta_i^*) \,, \\ r_\infty &= \frac{1}{n} \sum\nolimits_{j=1}^{n} \cos(\theta_i^*) \,. \end{aligned} \tag{40}$$

The equations (40) are solvable only if $K r_\infty \geq \|\omega\|_\infty$, and thus necessarily $r_\infty > 0$ unless $\omega = \mathbf{0}_n$. By eliminating θ^* from (40), we arrive at the *consistency equation*

$$r_\infty = \frac{1}{n} \sum\nolimits_{j=1}^{n} \pm\sqrt{1 - (\omega_i / K r_\infty)^2} \,, \tag{41}$$

where the $\pm$ signs are due to the equality: $\cos(\arcsin(x)) = \pm\sqrt{1-x^2}$ for $x \in \,]-1, 1[$. In fact, the consistency equation (41) is a set of 2^n equations corresponding to different possible equilibria θ^* in (40) and thus different choices of the $\pm$ signs, although not all choices yield feasible solutions $r_\infty \geq 0$. We refer to (Aeyels and Rogge, 2004) for a discussion of the consistency equation (41) and its infinite-dimensional counterpart (34). The implicit consistency equation (41) marks the starting point for the analyses in (Aeyels and Rogge, 2004; Mirollo and Strogatz, 2005; Verwoerd and Mason, 2008). By collecting various results in these three references, we arrive at the following statement, which has not been presented in this complete and self-contained form so far.

Theorem 6.5 (Implicit formulae for the exact critical coupling) *Consider the Kuramoto model* (2) *with* $n \geq 2$ *oscillators, natural frequencies* $\omega \in \mathbf{1}_n^\perp \setminus \{\mathbf{0}_n\}$, *and coupling strength* K. *Compute* $u^* \in [\|\omega\|_\infty, 2\|\omega\|_\infty]$ *as unique solution to the equation*

$$2 \sum\nolimits_{i=1}^{n} \sqrt{1 - (\omega_i/u)^2} = \sum\nolimits_{i=1}^{n} 1/\sqrt{1 - (\omega_i/u)^2} \,. \tag{42}$$

The following statements are equivalent:

(i) **Critical coupling:** *the coupling strength K is larger than a critical value, that is,*

$$K > K_{\text{critical}} \triangleq nu^* / \sum_{i=1}^{n} \sqrt{1-(\omega_i/u^*)^2}\,; \quad (43)$$

(ii) **Stable frequency synchronization:** *there exists at least one locally exponentially stable equilibrium manifold $[\theta^*] \in \mathbb{T}^n$.*

The implicit formulae (42)-(43) have been established by Verwoerd and Mason (2008, Theorem 3), who showed that K_{critical} is the smallest nonnegative value of the coupling strength for which the Kuramoto model (2) admits a frequency-synchronized solution. We remark that Verwoerd and Mason also extended the implicit formulae (42)-(43) to complete bipartite graphs (Verwoerd and Mason, 2009, Theorem 3) and infinite-dimensional networks (Verwoerd and Mason, 2011, Theorem 4). Moreover, they provided bisection algorithms to compute K_{critical} with predefined precision in a finite number of iterations. Aeyels and Rogge (2004) and Mirollo and Strogatz (2005) found similar implicit formulae and carried out a local stability analysis (Aeyels and Rogge, 2004, Theorems 1 and 3) and (Mirollo and Strogatz, 2005, Sections 3 and 4) showing a saddle-node bifurcation for $K = K_{\text{critical}}$: for $K < K_{\text{critical}}$ no frequency-synchronized solution (i.e., equilibrium manifolds) exists and for $K > K_{\text{critical}}$ a locally stable (corresponding to all + signs in (41)) and multiple unstable phase-locked solutions co-exist. As shown by Roberts (2008), the Kuramoto model (2) can be embedded into a higher-dimensional, linear, and complex-valued system, and the above stability results can also be elegantly established via linear systems theory, see (Conteville and Panteley, 2012).

Sufficient, explicit, and tight conditions: For the purpose of analyzing and selecting a sufficiently strong coupling in applications, Theorem 6.5 has three drawbacks. The stability results are local and the region of attraction of a synchronized solution is unknown. Second, the exact formulae (42)-(43) are implicit and thus not suited for performance estimates. For example, it is unclear which value of asymptotic arc invariance can be achieved if $K > c \cdot K_{\text{critical}}$ for some $c > 1$. Third and finally, the natural frequencies ω_i are often time-varying or uncertain in most applications. In this case, the exact value of K_{critical} needs to be estimated in continuous time, or a conservatively strong coupling $K \gg K_{\text{critical}}$ has to be chosen. The following theorem provides an explicit upper bound on the critical coupling together with performance estimates, convergence rates, and a guaranteed semi-global region of attraction. This bound is tight and thus necessary and sufficient when considering arbitrary distributions with compact support of the natural frequencies. The result has been originally presented in (Dörfler and Bullo, 2011, Theorem 4.1).

Theorem 6.6 (Explicit, sufficient, and tight critical coupling and practical phase sync) *Consider the Kuramoto model (2) with $n \geq 2$ oscillators, natural frequencies $\omega \in \mathbf{1}_n^\perp$ and coupling strength K. The following statements are equivalent:*

(i) **Critical coupling:** *the coupling strength K is larger than a critical value, that is,*

$$K > K_{\text{critical}} \triangleq \omega_{\max} - \omega_{\min}\,; \quad (44)$$

(ii) **Admissible initial arc invariance:** *there exists $\gamma_{\max} \in]\pi/2, \pi]$ such that the Kuramoto model (2) synchronizes exponentially for all possible distributions of the natural frequencies ω_i supported on the compact interval $[\omega_{\min}, \omega_{\max}]$ and for all initial phases $\theta(0) \in \text{Arc}_n(\gamma_{\max})$; and*

(iii) **Arc invariance of sync manifold:** *there exists $\gamma_{\min} \in [0, \pi/2[$ such that the Kuramoto model (2) has a locally exponentially stable synchronization manifold in $\overline{\text{Arc}}_n(\gamma_{\min})$ for all possible distributions of the natural frequencies ω_i supported on the compact interval $[\omega_{\min}, \omega_{\max}]$.*

If the equivalent conditions (i), (ii), and (iii) hold, then the ratio K_{critical}/K and the arc lengths $\gamma_{\min} \in [0, \pi/2[$ and $\gamma_{\max} \in]\pi/2, \pi]$ are related uniquely via $\sin(\gamma_{\min}) = \sin(\gamma_{\max}) = K_{\text{critical}}/K$. Moreover, the Kuramoto model (2) achieves **practical phase synchronization**, *that is, the set $\overline{\text{Arc}}_n(\gamma)$ is positively invariant for every $\gamma \in [\gamma_{\min}, \gamma_{\max}]$, and each trajectory originating in $\text{Arc}_n(\gamma_{\max})$ approaches asymptotically $\overline{\text{Arc}}_n(\gamma_{\min})$.*

The proof of Theorem 6.6 relies on the Jacobian and contraction properties developed in Subsections 4.1 and 5.2. If all angles at time $t \geq 0$ belong to a closed arc of length $\gamma \in [0, \pi[$, that is, $\theta(t) \in \overline{\text{Arc}}_n(\gamma)$, then the arc length $t \mapsto V(\theta(t))$ is non-increasing provided that

$$K \sin(\gamma) \geq \omega_{\max} - \omega_{\min}\,.$$

The above inequality holds true for $\gamma \in [\gamma_{\min}, \gamma_{\max}]$ if and only if condition (44) holds true. Additionally, $t \mapsto V(\theta(t))$ is strictly decreasing for $\gamma \in]\gamma_{\min}, \gamma_{\max}[$, the angles $\theta(t)$ reach the set $\overline{\text{Arc}}_n(\gamma_{\min}) \in \Delta_G(\pi/2)$, and frequency synchronization and stability follow from the results developed in Subsection 4.1. Hence, condition (44) implies properties (ii) and (iii) of Theorem 6.6. The converse implications follow since condition (44) is also necessary for synchronization with bipolar natural frequencies $\omega = \omega_{\text{bip}} \triangleq \omega_0 \cdot (-p \cdot \mathbf{1}_{n-p}, +(n-p) \cdot \mathbf{1}_p)$ with $\omega_0 \in \mathbb{R}$, $p \in \{1, \dots, n-1\}$, and for any of its permutations.

Besides establishing a tight condition for K_{critical}, Theorem 6.6 establishes some properties of the transient evolution of the Kuramoto dynamics (2) and shows that the

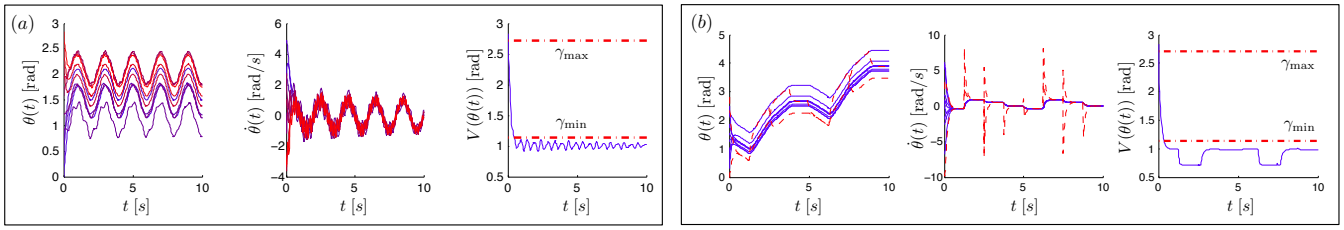

Fig. 14. Simulation of a network of $n = 10$ Kuramoto oscillators satisfying $K = 1.1 \cdot (\omega_{\max} - \omega_{\min})$. In panel (a), the natural frequencies $\omega_i : \mathbb{R}_{\geq 0} \to [\omega_{\min}, \omega_{\max}] = [0, 1]$ are smooth, bounded, and distinct sinusoidal functions. Each natural frequency $\omega_i(t)$ asymptotically converges to $\tilde{\omega}_i + \sin(\pi t)$ with constant and randomly chosen $\tilde{\omega}_i \in [0, 1]$. In panel (b), the natural frequencies $\omega_i(t)$ of oscillators 1 and 10 (displayed in red dashed lines) switch between constant values in $[\omega_{\min}, \omega_{\max}] = [0, 1]$. The simulations illustrate the phase cohesiveness of the angles $\theta(t)$ in $\overline{\mathrm{Arc}}_n(\gamma_{\min})$, the boundedness and convergence of the frequency variations (between consecutive switching instances) $\dot{\theta}(t) - \omega_{\mathrm{avg}}(t)\mathbf{1}_n$, as well as the monotonicity of the Lyapunov function $V(\theta(t))$ in $\overline{\mathrm{Arc}}_n(\gamma)$ for $\gamma \in [\gamma_{\min}, \gamma_{\max}]$.

asymptotic synchronization behavior of the Kuramoto model (2) is best described by the terminology *practical phase synchronization*, see also (Franci et al., 2011; Dörfler and Bullo, 2011). Notice also that Theorem 6.6 reduces to Theorem 5.2 for identical natural frequencies. We remark that similar analysis results are reported in (De Smet and Aeyels, 2007; Ha et al., 2010a; Choi et al., 2011a; Dörfler and Bullo, 2012b; Schmidt et al., 2012), and the bound $\gamma_{\min}$ on the ultimate phase distances can be improved for particular pairs of oscillators, see (Choi et al., 2011a, Theorem 5.2). Finally, we remark that the proof strategy via the contraction Lyapunov function (30) can be adapted to more general cases, for example, the conclusions of Theorem 6.6 can be extended to time-varying natural frequencies, see (Dörfler and Bullo, 2011) and the illustration in Figure 14.

Comparison and statistical analysis: Theorem 6.6 states the tight and explicit upper bound (44) on the critical coupling strength K_{critical}. Likewise, Lemma 6.4 states the tight and explicit lower bound (39) on K_{critical}. The exact critical coupling lies somewhere in-between and can be obtained from the implicit formulae (42)-(43). By collecting these results, we can state the following corollary, which improves upon the explicit bounds proposed by Verwoerd and Mason (2008, Corollary 7).

Corollary 6.7 (Tight explicit bounds) *Consider the Kuramoto model* (2) *with* $n \geq 2$ *oscillators, natural frequencies* $\omega \in \mathbf{1}_n^\perp \setminus \{\mathbf{0}_n\}$, *and coupling strength* K. *Compute the exact critical coupling* K_{critical} *according to* (42)-(43). *The explicit necessary condition* (39) *and sufficient condition* (44) *provide tight upper and lower bounds on the exact critical coupling* K_{critical}, *that is,*

$$\frac{n \cdot (\omega_{\max} - \omega_{\min})}{2\,(\sin(\gamma) + (n-2)\sin(\gamma/2))} \leq K_{\mathrm{critical}} \leq \omega_{\max} - \omega_{\min}\,, \tag{45}$$

where $\gamma \in [\pi/2, \pi]$ *is defined in* (38). *Moreover, the lower bound is tight for* $\omega = \omega_{\mathrm{trip}} \triangleq \omega_0 \cdot (+1, -1, \mathbf{0}_{n-1})$, *and the upper bound is tight for* $\omega = \omega_{\mathrm{bip}} \triangleq \omega_0 \cdot (-p \cdot \mathbf{1}_{n-p}, +(n-p) \cdot \mathbf{1}_p)$, *where* $\omega_0 \in \mathbb{R}$, $p \in \{1, \ldots, n-1\}$, *and both* ω_{trip} *and* ω_{bip} *are defined modulo index permutations.*

Corollary 6.7 is the finite-dimensional counterpart to Theorem 6.3 and identifies bipolar frequencies ω_{bip} and tripolar frequencies ω_{trip} as the extreme choices for the resulting critical coupling K_{critical}. These two distributions of natural frequencies are illustrated in Figure 13(a) and 13(e). We want to remark that for natural frequencies sampled from a particular distribution, $g(\omega)$, the critical quantity in Corollary 6.7, the support $\omega_{\max} - \omega_{\min}$, can be estimated by extreme value statistics, see (Bronski et al., 2012) for further details.

By Theorem 6.3, for infinite-dimensional models the uniform distribution $g_{\mathrm{unif}}(\omega) = 1/2$ yields the smallest synchronization threshold $K_{\mathrm{lock}} = 4\,\omega_0/\pi$ over all continuous, symmetric, and unimodal distributions $g(\omega)$ with bounded support $\omega \in [-\omega_0, +\omega_0]$. Hence, the uniform distribution is an interesting choice to compare the three conditions (39), (42)-(43), and (44) in a statistical analysis. Figure 15 reports our numerical findings. All three

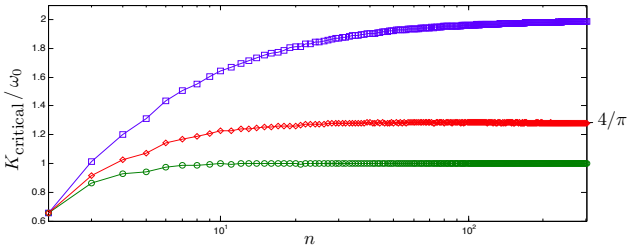

Fig. 15. Statistical analysis of the necessary, tight, and explicit bound (39) (◊), the exact and implicit formulae (42)-(43) (○), and the sufficient, tight, and explicit bound (44) (□) for $n \in [2, 300]$ oscillators, where the coupling gains for each n are averaged over 1000 samples of randomly uniformly generated frequencies.

displayed conditions are identical for $n = 2$ oscillators. As n increases, the sufficient bound (44) converges to the width $\omega_{\max} - \omega_{\min} = 2\omega_0$ of the support of $g_{\mathrm{unif}}(\omega)$, and the necessary bound (39) converges to half of that width. The exact value of K_{critical} given by (42)-(43) converges

to $4(\omega_{\max}-\omega_{\min})/(2\pi) = 4\omega_0/\pi$ in agreement with condition (35) predicted for the continuum limit.

7 Synchronization in Sparse Networks

This section considers the coupled oscillator model (1) in its general form featuring de-synchronizing dissimilar natural frequencies $\omega \in \mathbf{1}_n^\perp$ and the synchronizing coupling through a graph $G(\mathcal{V}, \mathcal{E}, A)$ with a nontrivial topology. The network science and physics communities coined the term *complex* for such non-trivial topologies to distinguish them from long-range (i.e., complete) and short-range (i.e., lattice-type) interaction topologies. The interest in such complex oscillator networks has been sparked by the seminal article (Jadbabaie et al., 2004) and the widespread scientific attention given to complex network studies (Strogatz, 2001; Boccaletti et al., 2006; Osipov et al., 2007; Arenas et al., 2008; Suykens and Osipov, 2008), and consensus and its applications (Olfati-Saber et al., 2007; Ren et al., 2007; Bullo et al., 2009; Garin and Schenato, 2010; Mesbahi and Egerstedt, 2010).

7.1 Survey of Synchronization Metrics and Conditions

Loosely speaking, the oscillator network (1) achieves synchronization when the coupling dominates the dissimilarity in natural frequencies. Various conditions have been proposed to quantify this trade-off for sparse graphs, both in theoretical studies as well as in power network applications. The coupling is typically quantified by the algebraic connectivity $\lambda_2(L)$ (Wu and Kumagai, 1980; Pecora and Carroll, 1998; Nishikawa et al., 2003; Jadbabaie et al., 2004; Restrepo et al., 2005; Boccaletti et al., 2006; Arenas et al., 2008; Dörfler and Bullo, 2012b; Motter et al., 2013), the weighted nodal degree $\deg_i = \sum_{j=1}^n a_{ij}$ (Wu and Kumagai, 1982; Korniss et al., 2006; Gómez-Gardeñes et al., 2007; Buzna et al., 2009; Dörfler and Bullo, 2012b, 2013; Skardal et al., 2013), or various metrics related to the notion of effective resistance (Wu and Kumagai, 1982; Korniss et al., 2006; Dörfler and Bullo, 2013). The frequency dissimilarity is quantified either by absolute norms $\|\omega\|_p$ or by incremental norms [8] $\|B^T\omega\|_p$, for $p \in \mathbb{N}$. Here, we specifically consider the three incremental norms:

$$\|\omega\|_{\mathcal{E},\infty} \triangleq \|B^T\omega\|_\infty = \max_{\{i,j\}\in\mathcal{E}} |\omega_i - \omega_j|\,,$$
$$\|\omega\|_{\mathcal{E},2} \triangleq \|B^T\omega\|_2 = \left(\sum\nolimits_{\{i,j\}\in\mathcal{E}} |\omega_i - \omega_2|^2\right)^{1/2},$$
$$\|\omega\|_{\mathcal{E}_{\text{cplt}},2} \triangleq \|B_{\text{cplt}}^T\omega\|_2 = \frac{1}{2}\left(\sum\nolimits_{i,j=1}^n |\omega_i - \omega_2|^2\right)^{1/2},$$

where the subscript cplt stands for the complete graph. With slight abuse of notation, we also adopt these incremental norms for angular differences. For example, for $\gamma \in [0, \pi[$, the incremental ∞-norm ball $\{\theta \in \mathbb{T}^n \mid \|\theta\|_{\mathcal{E}_\infty} \leq \gamma\}$ is identical to the phase cohesive set $\bar{\Delta}_G(\gamma)$.

As every review article on synchronization (Strogatz, 2000, 2001; Acebrón et al., 2005; Boccaletti et al., 2006; Arenas et al., 2008; Dörfler et al., 2013), let us state here that the problem of finding sharp and provably correct synchronization conditions is not yet completely solved. Some of the proposed synchronization conditions for complex oscillator networks can be evaluated only numerically since they are state-dependent (Wu and Kumagai, 1980, 1982) or arise from a non-trivial linearization process, such as the Master stability function formalism (Pecora and Carroll, 1998; Boccaletti et al., 2006; Arenas et al., 2008; Motter et al., 2013). In general, concise and accurate results are known only for specific topologies such as complete graphs (as discussed in the previous section), linear chains (Strogatz and Mirollo, 1988), highly symmetric ring graphs (Buzna et al., 2009), acyclic graphs (Dekker and Taylor, 2013), and complete bipartite graphs (Verwoerd and Mason, 2009) with uniform weights. For arbitrary coupling topologies, the literature contains only sufficient conditions (Wu and Kumagai, 1980, 1982; Jadbabaie et al., 2004; Dörfler and Bullo, 2012b) as well as numerical and statistical investigations for large random networks indicating certain (e.g. degree-dependent) scaling laws (Nishikawa et al., 2003; Restrepo et al., 2005; Gómez-Gardeñes et al., 2007; Moreno and Pacheco, 2004; Kalloniatis, 2010; Skardal et al., 2013). Numerical studies indicate that all known and provably-correct synchronization conditions are conservative estimates on the threshold from incoherence to synchrony. Our recently-proposed condition (Dörfler et al., 2013) is provably correct for various extremal network topologies and weights, and is numerically accurate for a broad range of random networks; a complete analytic treatment is missing at this time. In the following, we review a set of known and provably correct synchronization conditions and analysis concepts.

7.2 Sufficient Synchronization Conditions

For arbitrary network topologies and weights the equilibrium and potential energy landscape of the oscillator network (1) has been studied by different communities, see (Tavora and Smith, 1972a; Araposthatis et al., 1981; Baillieul and Byrnes, 1982; Mehta and Kastner, 2011). We particularly recommend the article (Araposthatis et al., 1981), where various surprising and counter-intuitive examples are reported. To the best of the authors' knowledge, the conditions (25)-(26) in Lemma 4.2 are the best known explicit necessary conditions for the existence of equilibria for arbitrary topolo-

[8] More precisely, the incremental norms $\|B^T\omega\|_p$ are *seminorms* in $\mathbb{R}^n$ and proper norms in $\mathbf{1}_n^\perp$.

gies and weights. In what follows, we focus on sufficient conditions guaranteeing frequency synchronization and we restrict ourselves to phase cohesive synchronous solutions within the set $\Delta_G(\pi/2)$. There are two reasons for this choice. First, as discussed in Subsection 4.1, the equilibria in $\Delta_G(\pi/2)$ are exponentially stable, and the forward invariance of the set $\Delta_G(\pi/2)$ leads to stable synchronization by incremental stability or frequency dynamics arguments. Second, from a pragmatic point of view, there are few analysis results and conditions for equilibria outside $\Delta_G(\pi/2)$, with the treatment of (directed) ring graphs in (Rogge and Aeyels, 2004; Ha and Kang, 2012) being a notable exception.

The approaches to phase synchronization (in Section 5) and to frequency synchronization in complete graphs (in Section 6) are generally not applicable to dissimilar natural frequencies and sparse coupling graphs, or are so only under very conservative conditions. For example, in the presence of dissimilar natural frequencies $\omega \in \mathbf{1}_n^\perp$, a Lyapunov analysis of the forced system (24) via the trigonometric potential function $U(\theta)$ is very involved since the level sets of $U(\theta)$ are hard to characterize. Likewise, the contraction Lyapunov analysis based on definition (30) inherently requires arc-invariance of *all* angles, and does not easily extend to arbitrary topologies. One quadratic Lyapunov function advocated by Jadbabaie et al. (2004); Chopra and Spong (2009) for classic Kuramoto oscillators (2) is $W : \mathrm{Arc}_n(\pi) \to \mathbb{R}$ defined by

$$W(\theta) = \frac{1}{4}\sum\nolimits_{i,j=1}^{n} |\theta_i - \theta_j|^2 = \frac{1}{2}\|\theta\|^2_{\mathcal{E}_{\mathrm{cplt}},2}\,. \tag{46}$$

This Lyapunov function is useful to analyze the more general oscillator network (1), and yields the following result found in (Dörfler and Bullo, 2012a, Theorem 4.6) and (Dörfler and Bullo, 2012b, Theorem 4.4).

Theorem 7.1 (Practical phase synchronization in sparse graphs I) *Consider the coupled oscillator model* (1) *with a connected graph* $G(\mathcal{V}, \mathcal{E}, A)$ *and frequencies* $\omega \in \mathbf{1}_n^\perp$. *There exists a locally exponentially stable equilibrium manifold* $[\theta] \in \Delta_G(\pi/2)$ *if the algebraic connectivity is larger than a critical value, that is,*

$$\lambda_2(L) > \lambda_{\mathrm{critical}} \triangleq \|\omega\|_{\mathcal{E}_{\mathrm{cplt}},2}\,. \tag{47}$$

Moreover, if condition (47) *holds, then the coupled oscillator model* (1) *achieves practical phase synchronization in the following sense. Given* $\gamma_{\max} \in]\pi/2, \pi]$ *and* $\gamma_{\min} \in [0, \pi/2[$ *as unique solutions to* $(\pi/2)\cdot\mathrm{sinc}(\gamma_{\max}) = \sin(\gamma_{\min}) = \lambda_{\mathrm{critical}}/\lambda_2(L)$, *the set* $\left\{\theta \in \mathrm{Arc}_n(\pi) \mid \|\theta\|^2_{\mathcal{E}_{\mathrm{cplt}},2} \leq \gamma\right\} \subseteq \bar{\Delta}_G(\gamma)$ *is positively invariant for all* $\gamma \in [\gamma_{\min}, \gamma_{\max}]$, *and each trajectory starting in* $\left\{\theta \in \mathrm{Arc}_n(\pi) \mid \|\theta\|^2_{\mathcal{E}_{\mathrm{cplt}},2} < \gamma_{\max}\right\}$ *asymptotically reaches* $\left\{\theta \in \mathrm{Arc}_n(\pi) \mid \|\theta\|^2_{\mathcal{E}_{\mathrm{cplt}},2} \leq \gamma_{\min}\right\}$.

The analysis leading to Theorem 7.1 is similar to the proof of Theorem 6.6: the Lyapunov function (46) is used to guarantee the ultimate boundedness of the phases in $\left\{\theta \in \mathrm{Arc}_n(\pi) \mid \|\theta\|_{\mathcal{E}_{\mathrm{cplt}},2} \leq \gamma_{\min}\right\} \subset \bar{\Delta}_G(\gamma_{\min})$, and the Jacobian arguments in Subsection 4.1 guarantee frequency synchronization. For classic Kuramoto oscillators (2), condition (47) reduces to $K > \|\omega\|_{\mathcal{E}_{\mathrm{cplt}},2}$; this condition is more conservative than the tight bound (44) which reads $K > \|\omega\|_{\mathcal{E},\infty} = \omega_{\max} - \omega_{\min}$. One reason for this conservatism is that condition (47) guarantees that *all* phase differences $|\theta_i - \theta_j|$ are bounded, not only those along the edges of the graph. However, by Lemma 4.1, we know that bounded phase differences $|\theta_i - \theta_j|$ *only* for $\{i, j\} \in \mathcal{E}$, are sufficient to establish the existence of a locally exponentially stable synchronized solution.

In what follows we adopt a fixed-point approach to the study of the equilibrium equations for the coupled oscillator model (1). In matrix notation, these equilibrium equations read as

$$\omega = B\mathcal{A}\,\mathbf{sin}(B^T\theta)\,, \tag{48}$$

where $\mathcal{A} = \mathrm{diag}(\{a_{ij}\}_{\{i,j\}\in\mathcal{E}})$ is the diagonal matrix of weights. We next follow the ingenious analysis of (48) suggested in (Jadbabaie et al., 2004, Section IIV.B). For the sake of a streamlined presentation, we treat the angles θ as vectors in $\mathbf{1}_n^\perp$. Recall the state-dependent weights $c_{ij}(\theta) = a_{ij}\,\mathrm{sinc}(\theta_i - \theta_j)$ from the consensus formulation (29), and define the state-dependent Laplacian $\mathcal{L}(\theta) = B\,\mathrm{diag}(\{c_{ij}(\theta)\}_{\{i,j\}\in\mathcal{E}})B^T$. Hence, equations (48) can be written compactly as $\omega = \mathcal{L}(\theta)\theta$. Since $\mathcal{L}(\theta)^\dagger \cdot \mathcal{L}(\theta) = I_n - \frac{1}{n}\mathbf{1}_{n\times n}$, we arrive at

$$\theta = \mathcal{L}(\theta)^\dagger\omega\,. \tag{49}$$

The following result has been obtained in (Dörfler and Bullo, 2012a, Theorem 4.7) by applying to equation (49) a fixed point theorem in the incremental two norm $\|\cdot\|_{\mathcal{E},2}$.

Theorem 7.2 (Practical phase synchronization in sparse graphs II) *Consider the coupled oscillator model* (1) *with a connected graph* $G(\mathcal{V}, \mathcal{E}, A)$ *and frequencies* $\omega \in \mathbf{1}_n^\perp$. *There exists a locally exponentially stable equilibrium manifold* $[\theta^*] \in \Delta_G(\pi/2)$ *if*

$$\lambda_2(L) > \lambda_{\mathrm{critical}} \triangleq \|\omega\|_{\mathcal{E},2}\,. \tag{50}$$

Moreover, if condition (50) *holds, then* $[\theta^*]$ *is phase cohesive in the following sense:* $[\theta^*] \in \{\theta \in \mathbb{T}^n \mid \|\theta\|_{\mathcal{E},2} \leq \gamma_{\min}\} \subseteq \bar{\Delta}_G(\gamma_{\min})$, *where* $\gamma_{\min} \in [0, \pi/2[$ *satisfies* $\sin(\gamma_{\min}) = \lambda_{\mathrm{critical}}/\lambda_2(L)$.

Clearly, condition (50) is sharper than condition (47), but the stability result is only local. The synchronization condition (50) is the sharpest sufficient condition for general graphs known to the authors, but it is still a conservative estimate for most network topologies and

weights. Indeed, the necessary condition (26) and sufficient condition (50) are separated by a tremendous gap for $n > 2$ oscillators. The reasons for this conservatism are manifold. First, condition (50) guarantees the bound $\|\theta^*\|_{\mathcal{E},2} \leq \arcsin(\lambda_{\text{critical}}/\lambda_2(L))$. This incremental 2-norm bound is a very strong property, and only the incremental ∞-norm $\|\theta\|_{\mathcal{E},\infty}$ needs to be bounded to conclude synchronization by Lemma 4.1. Second, the derivation of the conditions (25), (26), (47), and (50) involves conservative bounding of the trigonometric nonlinearities and network interactions. Third, Lemma 4.1, Theorem 5.2, and Theorem 6.6 hint at the incremental ∞-norm as a natural metric, whereas an analysis using 2-norm type metrics inherently leads to more conservative results.

7.3 Towards an Exact Synchronization Condition

An analysis of the fixed-point equations (49) using 2-norm bounding of $\|\mathcal{L}(\theta)^\dagger\omega\|_{\mathcal{E},2}$ results in the condition $\|\omega\|_{\mathcal{E},2}/\lambda_2(L) < 1$ in Theorem 7.2. As discussed above, an ∞-norm analysis of equations (49) and the term $\|\mathcal{L}(\theta)^\dagger\omega\|_{\mathcal{E},\infty}$ should yield a less conservative condition, possibly of the form $\|L^\dagger\omega\|_{\mathcal{E},\infty} < 1$. Indeed, this condition can be derived for particular networks. By formally replacing each term $\sin(\theta_i - \theta_j)$ in the fixed-point equations (48) by an auxiliary scalar variable ψ_{ij} we arrive at

$$\omega = B\mathcal{A}\psi\,, \tag{51}$$
$$\psi = \mathbf{sin}(B^T\theta)\,, \tag{52}$$

where $\psi \in \mathbb{R}^{|\mathcal{E}|}$ is a vector with elements ψ_{ij}. We refer to equations (51) as the *auxiliary-fixed point equation*. It can be easily verified that every solution of the auxiliary fixed-point equations (51) is of the form

$$\psi = B^T L^\dagger\omega + \psi_{\text{hom}}\,, \tag{53}$$

where the homogeneous solution $\psi_{\text{hom}} \in \mathbb{R}^{|\mathcal{E}|}$ satisfies $\mathcal{A}\psi_{\text{hom}} \in \operatorname{Ker}(B)$. Since the orthogonal vector spaces $\operatorname{Ker}(B)$ and $\operatorname{Ker}(B)^\perp = \operatorname{Im}(B^T)$ are spanned by vectors associated to cycles and cutsets in the graph, see (Biggs, 1994, 1997), we arrive at the following characterization of the fixed points (Dörfler et al., 2013, Theorem 1).

Lemma 7.3 (Properties of the fixed point equations) *Consider the coupled oscillator model* (1) *with graph* $G(\mathcal{V},\mathcal{E},A)$ *and* $\omega \in \mathbf{1}_n^\perp$*, its fixed-point equations* (48)*, and the auxiliary fixed-point equations* (51)*. Let* $\gamma \in [0,\pi/2[$*. The following statements are equivalent:*

(i) There exists a solution $\theta^* \in \bar{\Delta}_G(\gamma)$ *to the fixed-point equations* (48)*; and*
(ii) There exists a solution $\psi \in \mathbb{R}^{|\mathcal{E}|}$ *to the auxiliary fixed-point equation* (51) *of the form* (53) *satisfying the norm constraint* $\|\psi\|_\infty \leq \sin(\gamma)$ *and the cycle constraint* $\mathbf{arcsin}(\psi) \in \operatorname{Im}(B^T)$.

If the equivalent statements (i) and (ii) are true, then we have $B^T\theta^* = \mathbf{arcsin}(\psi)$*. Additionally,* $[\theta^*] \in \bar{\Delta}_G(\gamma)$ *is a locally exponentially stable synchronization manifold.*

By Lemma 7.3, the cycle space $\operatorname{Ker}(B)$ of the graph serves as a degree of freedom to find a minimum ∞-norm solution $\psi^* \in \mathbb{R}^{|\mathcal{E}|}$ to equations (51), which yields an *optimal* necessary synchronization condition.

Corollary 7.4 (Optimal necessary synchronization condition) *Consider the coupled oscillator model* (1) *with a connected graph* $G(\mathcal{V},\mathcal{E},A)$ *and* $\omega \in \mathbf{1}_n^\perp$*. Compute* $\psi^* \in \mathbb{R}^{|\mathcal{E}|}$ *as solution to the optimization problem*

$$\text{minimize}_{\psi\in\mathbb{R}^{|\mathcal{E}|}}\ \|\psi\|_\infty \quad s.t. \quad \omega = B\mathcal{A}\psi. \tag{54}$$

Let $\gamma \in [0,\pi/2[$*. There exists a locally exponentially stable equilibrium manifold* $[\theta^*] \in \bar{\Delta}_G(\gamma)$ *only if* $\|\psi^*\|_\infty \leq \sin(\gamma)$*.*

If the graph is acyclic, then there are no cycle constraints, and the norm constraint in Lemma 7.3 reduces to $\sin(\gamma) \geq \|\psi\|_\infty = \|L^\dagger\omega\|_{\mathcal{E},\infty}$. We arrive at the following corollary (Dörfler et al., 2013, Theorem 2).

Corollary 7.5 (Practical phase synchronization in acyclic graphs) *Consider the coupled oscillator model* (1) *with a connected and acyclic graph* $G(\mathcal{V},\mathcal{E},A)$ *and* $\omega \in \mathbf{1}_n^\perp$*. There exists a locally exponentially stable equilibrium manifold* $[\theta^*] \in \Delta_G(\pi/2)$ *if and only if*

$$\|L^\dagger\omega\|_{\mathcal{E},\infty} < 1\,. \tag{55}$$

Moreover, if condition (55) *holds, then* $[\theta^*]$ *is phase cohesive in* $\bar{\Delta}_G(\gamma_{\min})$*, where* $\gamma_{\min} \in [0,\pi/2[$ *satisfies* $\sin(\gamma_{\min}) = \|L^\dagger\omega\|_{\mathcal{E},\infty}$*.*

Condition (55) is equivalent to the cutset condition (Dekker and Taylor, 2013, Lemma 1). Dörfler et al. (2013) also proved that condition (55) is sufficient and tight for various extremal graph topologies and parameters such as complete and uniformly weighted graphs (in this case (55) is equivalent to (44)), small cycles of length strictly less than five, cutset-inducing natural frequencies $\omega = L\omega_{\text{bip}}$, in the limit $\|L^\dagger\omega\|_{\mathcal{E},\infty} \searrow 0$, and 1-connected combinations of these graphs. Moreover, by means of a statistical analysis, it can be shown that condition (55) is extremely accurate for a broad set of random network topologies and weights as well as for standard power network test cases. However, the authors also identified possibly thin sets of network topologies and parameters for which condition (55) is not sufficiently tight.

We conclude this section with a comparison of the synchronization conditions (25), (26), (47), (50), and (55).

Let $V \in \mathbb{R}^{n\times n}$ be the matrix of orthonormal eigenvectors of L and let $0 = \lambda_1 < \lambda_2 \leq \cdots \leq \lambda_n$ be the corresponding eigenvalues. Then condition (55) reads as

$$\left\| V \operatorname{diag}\left(0, 1/\lambda_2, \ldots, 1/\lambda_n\right) \cdot \left(V^T \omega\right) \right\|_{\mathcal{E},\infty} < 1 \,. \quad (56)$$

A sufficient condition for inequality (56) is $\lambda_2 > \|\omega\|_{\mathcal{E},\infty}$, which strictly improves upon the algebraic connectivity conditions (47) and (50). Likewise, a necessary condition for (56) is $2 \cdot \max_{i\in\mathcal{V}} \deg_i \geq \lambda_n \geq \|\omega\|_{\mathcal{E},\infty}$, resembling the degree-dependent conditions (25) and (26). When compared to (56), this sufficient condition and this necessary condition feature only one of $n-1$ nonzero Laplacian eigenvalues and are overly conservative. We conclude that condition (55) strongly improves upon the conditions (25), (26), (47), and (50), but a complete analytic characterization of its applicability is still open.

8 Conclusions and Open Research Directions

In this paper we introduced the reader to the coupled oscillator model (1), we reviewed several applications, we discussed different synchronization notions, and we presented different analysis approaches and results for phase synchronization, phase balancing, pattern formation, and frequency synchronization. We covered complete and sparse network topologies, homogeneous and heterogeneous natural frequencies, and finite and infinite oscillator populations.

Despite the vast literature, the countless applications, and the numerous theoretical results on the synchronization properties of model (1), many interesting and important problems are still open. In the following, we summarize limitations of the existing analysis approaches and present a few worthwhile directions for future research.

Asymmetric interactions: Most of the results presented in this paper can be extended to more general anti-symmetric and 2π-periodic coupling functions as long as the coupling is diffusive and bidirectional. In some applications, the coupling topology is inherently directed, such as transcriptional, metabolic, or neuronal networks (Mason and Verwoerd, 2007). In this case, there are only a few theoretical investigations including ring graphs (Rogge and Aeyels, 2004; Ha and Kang, 2012), results on the synchronization frequency (Ati and Panteley, 2012; Dörfler and Bullo, 2012b), and statistical analysis of large graphs (Restrepo et al., 2006). Also, in many applications the coupling between the oscillators is not purely diffusive. For instance, mutual excitatory or inhibitory synaptic organizations in neuroscience (Crook et al., 1997), time delays in sensor networks (Simeone et al., 2008), or transfer conductances in power networks (Chiang et al., 1995) lead to a shifted coupling of the form $\sin(\theta_i - \theta_j - \varphi_{ij})$ with $\varphi_{ij} \in [-\pi/2, \pi/2]$. In these cases and also for other "skewed" or "symmetry-breaking" interactions among the oscillators, many of the presented analysis schemes either fail completely or lead to overly conservative results.

Pulse coupling: Another interesting class of oscillator networks are systems of pulse-coupled oscillators featuring hybrid dynamics: impulsive coupling at discrete time instants and uncoupled continuous dynamics otherwise. This class of oscillator networks displays a very interesting phenomenology which is qualitatively different from diffusive and continuous coupling, see (Mauroy et al., 2012). For instance, the behavior of identical oscillators coupled in a complete graph strongly depends on the curvature of the uncoupled dynamics. As discussed in Subsection 2.4, such pulse-coupled oscillator models can be reduced to the canonical model (12) through a phase reduction and averaging analysis. For certain pulse-coupled oscillators the coupling functions $h_{ij}(\cdot)$ turn out to be monotone and discontinuous, and they result in finite-time convergent dynamics (Mauroy and Sepulchre, 2012; Kuramoto, 1991). Most of the results and analysis methods known for continuously-coupled oscillators still need to be extended to pulse-coupled oscillators, especially in the case of dissimilar natural frequencies.

Transient dynamics: For dissimilar oscillators, most results presented in this paper pertain to existence and local stability of synchronous solutions, with the exception of Theorems 6.6 and 7.1. Even for the Kuramoto model (2), many problems pertaining to the transient dynamics still need to be fully resolved. For instance, most known estimates on the region of attraction of a synchronized solution are conservative, such as the semi-circle estimates given in Theorems 5.2 and 6.6. We refer to (Chiang et al., 1995; Wiley et al., 2006) for a set of interesting results and conjectures on the region of attraction. As shown in Theorem 6.6, for complete graphs, the region of attraction of a synchronous solution always includes $\Delta_G(\pi/2)$ for any $K > K_{\text{critical}}$. It is unclear if an analogous result holds for sparse graphs or if the region of attraction severely depends on the topology. When the Kuramoto dynamics (2) are subject to additive noise, they can be analyzed through Fokker-Planck equations similar to the continuum-limit model (16)-(17) or in the limit of small stochastic perturbations, see (Bag et al., 2007; DeVille, 2011). In this case, there are various interesting transitions between wells of the potential landscape and only few analytic investigations. Also the sub-synchronous regime for $K < K_{\text{critical}}$ is vastly unexplored, and partial synchronization or clustering (similar to the partially-synchronized state for infinite-dimensional models) (Aeyels and Rogge, 2004; De Smet and Aeyels, 2007) or chaotic motion (Maistrenko et al., 2005; Tönjes, 2007; Popovych et al., 2005; Suykens and Osipov, 2008) can occur. Finally, the incremental stability results referenced in Subsection 4.1 appear to be a promising direction that still needs to be fully explored.

Higher-order and state space oscillators: For the mechanical analog in Figure 1 and the previously listed applications (Bergen and Hill, 1981; Ermentrout, 1991; Chiang et al., 1995; Sauer and Pai, 1998; Wiesenfeld et al., 1998; Hoppensteadt and Izhikevich, 2000; Bennett et al., 2002; Pantaleone, 2002; Strogatz et al., 2005; Righetti and Ijspeert, 2006; Shim et al., 2007; Ha et al., 2010b, 2011; Kapitaniak et al., 2012; Zhang et al., 2012) the coupled oscillator dynamics are not exactly given by the first-order phase model (1). In many cases, the dynamics are of second order as in (7). The analysis of second-order oscillator networks has also received a lot of attention, see (Acebrón et al., 2005; Dörfler and Bullo, 2011; Choi et al., 2011b) for a literature overview. Among others, the contraction Lyapunov function (30) can be extended to second-order oscillators (Choi et al., 2011b), the continuum-limit analysis can be extended (Acebrón et al., 2005), and the local stability properties are preserved when going from first to second order (Dörfler and Bullo, 2011). Of course, the transient dynamics of second-order oscillator networks have their own characteristics, especially for large inertia and small damping (Paganini and Lesieutre, 1999). Thus, many of the presented results still need to be extended to second-order oscillator networks. In other instances of oscillator networks, there is no readily available phase variable to describe the limit cycle dynamics of the coupled system, and the model (1) is valid only after a phase reduction and averaging analysis. Since features of the original model may be poorly preserved in the canonical model (12), a direct analysis of the state space model is preferred. In the case of linear or passive systems, state or output synchronization are well understood (Arcak, 2007; Wieland, 2010; Bürger et al., 2012; Lunze, 2012), but the analysis of synchronization problems in more general heterogeneous state space oscillator networks remains a challenging and important problem.

Sparse and heterogeneous networks: Despite the vast scientific interest the quest for sharp, concise, and closed-form synchronization conditions for arbitrary connected graphs has been so far in vain. As suggested by our discussion in Section 7, the proper metric for the analysis of synchronization problem appears to be the incremental ∞-norm. In the authors' opinion, an analysis with the incremental ∞-norm will most likely deliver the sharpest possible conditions. We believe that the norm and cycle constraints developed in (Dörfler et al., 2013) are a fruitful approach towards a more complete understanding of sparse topologies. Likewise, for the transient analysis, the ℓ_∞-type contraction Lyapunov function (30) is a powerful analysis concepts for complete graphs and still needs to be extended to arbitrary connected graphs. Regarding the potential and equilibrium landscape, a few interesting and still unresolved conjectures can be found in (Tavora and Smith, 1972a; Araposthatis et al., 1981; Baillieul and Byrnes, 1982; Mehta and Kastner, 2011) and pertain to the number of (stable) equilibria and topological properties of the equilibrium set. Finally, the complex networks and statistical physics communities found various interesting scaling laws in their statistical and numerical analyses of random graph models, such as conditions depending on the spectral ratio λ_2/λ_n of the Laplacian eigenvalues, interesting results for correlations between the degree $\deg_i$ and the natural frequency ω_i, and degree-dependent synchronization conditions (Nishikawa et al., 2003; Moreno and Pacheco, 2004; Restrepo et al., 2005; Boccaletti et al., 2006; Gómez-Gardeñes et al., 2007; Arenas et al., 2008; Kalloniatis, 2010; Skardal et al., 2013). It is unclear which of these results and findings are amenable to an analytic and quantitative investigation.

We sincerely hope that this survey article stimulates further exciting research on synchronization in coupled oscillators, both on the theoretical side as well as in the countless applications.

References

Abidi, A. A., Chua, L. O., 1979. On the dynamics of Josephson-junction circuits. IEE Journal on Electronic Circuits and Systems 3 (4), 186–200.

Acebrón, J. A., Bonilla, L. L., Vicente, C. J. P., Ritort, F., Spigler, R., 2005. The Kuramoto model: A simple paradigm for synchronization phenomena. Reviews of Modern Physics 77 (1), 137–185.

Adler, R., 1946. A study of locking phenomena in oscillators. Proceedings of the IRE 34 (6), 351–357.

Aeyels, D., Rogge, J. A., 2004. Existence of partial entrainment and stability of phase locking behavior of coupled oscillators. Progress on Theoretical Physics 112 (6), 921–942.

Angeli, D., 2002. A Lyapunov approach to incremental stability properties. IEEE Transactions on Automatic Control 47 (3), 410–421.

Aoi, S., Tsuchiya, K., 2005. Locomotion control of a biped robot using nonlinear oscillators. Autonomous Robots 19 (3), 219–232.

Araposthatis, A., Sastry, S., Varaiya, P., 1981. Analysis of power-flow equation. International Journal of Electrical Power & Energy Systems 3 (3), 115–126.

Arcak, M., 2007. Passivity as a design tool for group coordination. IEEE Transactions on Automatic Control 52 (8), 1380–1390.

Arcak, M., Dec. 2012. Synchronization and pattern formation in diffusively coupled systems. In: IEEE Conf. on Decision and Control. Maui, HI, USA, pp. 7184–7192.

Arenas, A., Díaz-Guilera, A., Kurths, J., Moreno, Y., Zhou, C., 2008. Synchronization in complex networks. Physics Reports 469 (3), 93–153.

Ati, A. E., Panteley, E., Mar. 2012. On frequency synchronization of kuramoto model with non-symmetric interconnection structure. In: Int. Conf. on Communications, Computing and Control Applications. Hammamet, Tunisia.

Bag, B. C., Petrosyan, K. G., Hu, C. K., 2007. Influence of noise on the synchronization of the stochastic Kuramoto model. Physical Review E 76 (5), 056210.

Baillieul, J., Byrnes, C. I., 1982. Geometric critical point analysis of lossless power system models. IEEE Transactions on Circuits and Systems 29 (11), 724–737.

Baldoni, R., Corsaro, A., Querzoni, L., Scipioni, S., Piergiovanni, S. T., 2010. Coupling-based internal clock synchronization for large-scale dynamic distributed systems. IEEE Transactions on Parallel and Distributed Systems 21 (5), 607–619.

Balmforth, N. J., Sassi, R., 2000. A shocking display of synchrony. Physica D: Nonlinear Phenomena 143 (1), 21–55.

Barbarossa, S., Scutari, G., 2007. Decentralized maximum-likelihood estimation for sensor networks composed of nonlinearly coupled dynamical systems. IEEE Transactions on Signal Processing 55 (7), 3456–3470.

Bennett, M., Schatz, M. F., Rockwood, H., Wiesenfeld, K., 2002. Huygens's clocks. Proceedings: Mathematical, Physical and Engineering Sciences 458 (2019), 563–579.

Bergen, A. R., Hill, D. J., 1981. A structure preserving model for power system stability analysis. IEEE Transactions on Power Apparatus and Systems 100 (1), 25–35.

Biggs, N., 1994. Algebraic Graph Theory, 2nd Edition. Cambridge University Press.

Biggs, N., 1997. Algebraic potential theory on graphs. Bulletin of the London Mathematical Society 29 (6), 641–683.

Boccaletti, S., Latora, V., Moreno, Y., Chavez, M., Hwang, D. U., 2006. Complex networks: Structure and dynamics. Physics Reports 424 (4-5), 175–308.

Bronski, J. C., DeVille, L., Jip Park, M., 2012. Fully synchronous solutions and the synchronization phase transition for the finite-n Kuramoto model. Chaos: An Interdisciplinary Journal of Nonlinear Science 22 (3), 033133.

Brown, E., Holmes, P., Moehlis, J., 2003. Globally coupled oscillator networks. In: Kaplan, E., Marsden, J. E., Sreenivasan, K. R. (Eds.), Perspectives and Problems in Nonlinear Science: A Celebratory Volume in Honor of Larry Sirovich. Springer, pp. 183–215.

Brown, E., Moehlis, J., Holmes, P., 2004. On the phase reduction and response dynamics of neural oscillator populations. Neural Computation 16 (4), 673–715.

Buck, J., 1988. Synchronous rhythmic flashing of fireflies. II. Quarterly Review of Biology 63 (3), 265–289.

Bullo, F., Cortés, J., Martínez, S., 2009. Distributed Control of Robotic Networks. Princeton University Press.

Bürger, M., Zelazo, D., Allgöwer, F., 2012. Hierarchical clustering of dynamical networks using a saddle-point analysis. IEEE Transactions on Automatic ControlTo appear.

Buzna, L., Lozano, S., Diaz-Guilera, A., 2009. Synchronization in symmetric bipolar population networks. Physical Review E 80 (6), 66120.

Canale, E., Monzón, P., 2008. Almost global synchronization of symmetric Kuramoto coupled oscillators. In: Systems Structure and Control. InTech Education and Publishing, Ch. 8, pp. 167–190.

Canale, E. A., Monzón, P., Robledo, F., Dec. 2010a. On the complexity of the classification of synchronizing graphs. In: Grid and Distributed Computing, Control and Automation. Jeju Island, Korea, pp. 186–195.

Canale, E. A., Monzón, P. A., Robledo, F., Jun. 2010b. The wheels: an infinite family of bi-connected planar synchronizing graphs. In: IEEE Conf. Industrial Electronics and Applications. Taichung, Taiwan, pp. 2204–2209.

Chandrashekhar, K. S., Hill, D. J., 1986. Cutset stability criterion for power systems using a structure-preserving model. International Journal of Electrical Power & Energy Systems 8 (3), 146–157.

Chiang, H.-D., Chu, C. C., Cauley, G., 1995. Direct stability analysis of electric power systems using energy functions: Theory, applications, and perspective. Proceedings of the IEEE 83 (11), 1497–1529.

Chiba, H., Aug. 2010. A proof of the Kuramoto's conjecture for a bifurcation structure of the infinite dimensional Kuramoto model. Available at `http://arxiv.org/abs/1008.0249`.

Choi, Y. P., Ha, S. Y., Jung, S., Kim, Y., 2011a. Asymptotic formation and orbital stability of phase-locked states for the Kuramoto model. Physica D: Nonlinear Phenomena 241 (7), 735–754.

Choi, Y.-P., Ha, S.-Y., Yun, S.-B., 2011b. Complete synchronization of Kuramoto oscillators with finite inertia. Physica D 240 (1), 32–44.

Chopra, N., Spong, M. W., 2009. On exponential synchronization of Kuramoto oscillators. IEEE Transactions on Automatic Control 54 (2), 353–357.

Chung, S. J., Slotine, J. J., Dec. 2010. On synchronization of coupled Hopf-Kuramoto oscillators with phase delays. In: IEEE Conf. on Decision and Control. Atlanta, GA, USA, pp. 3181–3187.

Conteville, L., Panteley, E., Mar. 2012. Linear reformulation of the Kuramoto model: Asymptotic mapping and stability properties. In: Int. Conf. on Communications, Computing and Control Applications. Hammamet, Tunisia.

Crawford, J. D., 1994. Amplitude expansions for instabilities in populations of globally-coupled oscillators. Journal of statistical physics 74 (5), 1047–1084.

Crook, S. M., Ermentrout, G. B., Vanier, M. C., Bower, J. M., 1997. The role of axonal delay in the synchronization of networks of coupled cortical oscillators. Journal of Computational Neuroscience 4 (2), 161–172.

Cross, M. C., Hohenberg, P. C., 1993. Pattern formation outside of equilibrium. Reviews of Modern Physics 65 (3), 851.

Daido, H., 1992. Quasientrainment and slow relaxation in a population of oscillators with random and frustrated interactions. Physical Review Letters 68 (7),

1073–1076.
De Smet, F., Aeyels, D., 2007. Partial entrainment in the finite Kuramoto–Sakaguchi model. Physica D: Nonlinear Phenomena 234 (2), 81–89.
Dekker, A. H., Taylor, R., 2013. Synchronization properties of trees in the Kuramoto model. SIAM Journal on Applied Dynamical Systems 12 (2), 596–617.
DeVille, L., 2011. Transitions amongst synchronous solutions for the stochastic Kuramoto model. Nonlinearity 25 (5), 1–20.
Do, A. L., Boccaletti, S., Gross, T., 2012. Graphical notation reveals topological stability criteria for collective dynamics in complex networks. Physical Review Letters 108 (19), 194102.
Dörfler, F., Bullo, F., 2011. On the critical coupling for Kuramoto oscillators. SIAM Journal on Applied Dynamical Systems 10 (3), 1070–1099.
Dörfler, F., Bullo, F., Dec. 2012a. Exploring synchronization in complex oscillator networks. In: IEEE Conf. on Decision and Control. Maui, HI, USA, pp. 7157–7170.
Dörfler, F., Bullo, F., 2012b. Synchronization and transient stability in power networks and non-uniform Kuramoto oscillators. SIAM Journal on Control and Optimization 50 (3), 1616–1642.
Dörfler, F., Bullo, F., 2013. Kron reduction of graphs with applications to electrical networks. IEEE Transactions on Circuits and Systems I: Regular Papers 60 (1), 150–163.
Dörfler, F., Chertkov, M., Bullo, F., 2013. Synchronization in complex oscillator networks and smart grids. Proceedings of the National Academy of Sciences 110 (6), 2005–2010.
Ermentrout, G. B., 1985. Synchronization in a pool of mutually coupled oscillators with random frequencies. Journal of Mathematical Biology 22 (1), 1–9.
Ermentrout, G. B., 1991. An adaptive model for synchrony in the firefly *pteroptyx malaccae*. Journal of Mathematical Biology 29 (6), 571–585.
Ermentrout, G. B., Kopell, N., 1984. Frequency plateaus in a chain of weakly coupled oscillators, I. SIAM Journal on Mathematical Analysis 15 (2), 215–237.
Filatrella, G., Nielsen, A. H., Pedersen, N. F., 2008. Analysis of a power grid using a Kuramoto-like model. The European Physical Journal B 61 (4), 485–491.
Fioriti, V., Ruzzante, S., Castorini, E., Marchei, E., Rosato, V., 2009. Stability of a distributed generation network using the Kuramoto models. In: Critical Information Infrastructure Security. Lecture Notes in Computer Science. Springer, pp. 14–23.
Forni, F., Sepulchre, R., 2012. A differential Lyapunov framework for contraction analysis. Available at `http://arxiv.org/abs/1208.2943`.
Franci, A., Chaillet, A., Pasillas-Lépine, W., 2011. Existence and robustness of phase-locking in coupled Kuramoto oscillators under mean-field feedback. Automatica 47 (6), 1193–1202.
Garin, F., Schenato, L., 2010. A survey on distributed estimation and control applications using linear consensus algorithms. In: Bemporad, A., Heemels, M., Johansson, M. (Eds.), Networked Control Systems. LNCIS. Springer, pp. 75–107.
Ghosh, A. K., Chance, B., Pye, E. K., 1971. Metabolic coupling and synchronization of NADH oscillations in yeast cell populations. Archives of Biochemistry and Biophysics 145 (1), 319–331.
Gómez-Gardeñes, J., Moreno, Y., Arenas, A., 2007. Paths to synchronization on complex networks. Physical Review Letters 98 (3), 34101.
Ha, S., Lattanzio, C., Rubino, B., Slemrod, M., 2011. Flocking and synchronization of particle models. Quarterly Applied Mathematics 69, 91–103.
Ha, S.-Y., Ha, T., Kim, J.-H., 2010a. On the complete synchronization of the Kuramoto phase model. Physica D: Nonlinear Phenomena 239 (17), 1692–1700.
Ha, S. Y., Jeong, E., Kang, M. J., 2010b. Emergent behaviour of a generalized Viscek-type flocking model. Nonlinearity 23 (12), 3139–3156.
Ha, S. Y., Kang, M. J., 2012. On the basin of attractors for the unidirectionally coupled Kuramoto model in a ring. SIAM Journal on Applied Mathematics 72 (5), 1549–1574.
Ha, S. Y., Slemrod, M., 2011. A fast-slow dynamical systems theory for the Kuramoto type phase model. Journal of Differential Equations 251 (10), 2685–2695.
Hill, D. J., Chen, G., May 2006. Power systems as dynamic networks. In: IEEE Int. Symposium on Circuits and Systems. Kos, Greece, pp. 722–725.
Hong, Y. W., Scaglione, A., 2005. A scalable synchronization protocol for large scale sensor networks and its applications. IEEE Journal on Selected Areas in Communications 23 (5), 1085–1099.
Hoppensteadt, F. C., Izhikevich, E. M., 1997. Weakly Connected Neural Networks. Springer.
Hoppensteadt, F. C., Izhikevich, E. M., 2000. Synchronization of laser oscillators, associative memory, and optical neurocomputing. Physical Review E 62 (3), 4010–4013.
Hoppensteadt, F. C., Izhikevich, E. M., 2001. Synchronization of MEMS resonators and mechanical neurocomputing. IEEE Transactions on Circuits and Systems I: Fundamental Theory and Applications 48 (2), 133–138.
Huepe, C., Cadiz, R. F., Colasso, M., Jun. 2012. Generating music from flocking dynamics. In: American Control Conference. Montréal, Canada, pp. 4339–4344.
Huygens, C., 1893. Oeuvres Complètes De Christiaan Huygens. Societe Hollandaise des Sciences, The Hague, Netherlands, m. Nijhoff, ed.
Ijspeert, A. J., 2008. Central pattern generators for locomotion control in animals and robots: A review. Neural Networks 21 (4), 642–653.
Izhikevich, E. M., 2007. Dynamical Systems in Neuroscience: The Geometry of Excitability and Bursting. MIT Press.
Izhikevich, E. M., Kuramoto, Y., 2006. Weakly coupled oscillators. Encyclopedia of Mathematical Physics 5,

448.
Jadbabaie, A., Motee, N., Barahona, M., Jun. 2004. On the stability of the Kuramoto model of coupled nonlinear oscillators. In: American Control Conference. Boston, MA, USA, pp. 4296–4301.
Jongen, G., Anemüller, J., Bollé, D., Coolen, A. C. C., Perez-Vicente, C., 2001. Coupled dynamics of fast spins and slow exchange interactions in the XY spin glass. Journal of Physics A: Mathematical and General 34 (19), 3957–3984.
Justh, E. W., Krishnaprasad, P. S., 2004. Equilibria and steering laws for planar formations. Systems & Control Letters 52 (1), 25–38.
Kalloniatis, A. C., 2010. From incoherence to synchronicity in the network Kuramoto model. Physical Review E 82 (6), 066202.
Kapitaniak, M., Czolczynski, K., Perlikowski, P., Stefanski, A., Kapitaniak, T., 2012. Synchronization of clocks. Physics Reports 517, 1–69.
Khalil, H. K., 2002. Nonlinear Systems, 3rd Edition. Prentice Hall.
Kiss, I. Z., Zhai, Y., Hudson, J. L., 2002. Emerging coherence in a population of chemical oscillators. Science 296 (5573), 1676–1678.
Klein, D. J., 2008. Coordinated control and estimation for multi-agent systems: Theory and practice. Ph.D. thesis, University of Washington.
Klein, D. J., Lee, P., Morgansen, K. A., Javidi, T., 2008. Integration of communication and control using discrete time Kuramoto models for multivehicle coordination over broadcast networks. IEEE Journal on Selected Areas in Communications 26 (4), 695–705.
Kopell, N., Ermentrout, G. B., 1988. Coupled oscillators and the design of central pattern generators. Mathematical Biosciences 90 (1-2), 87–109.
Korniss, G., Hastings, M. B., Bassler, K. E., Berryman, M. J., Kozma, B., Abbott, D., 2006. Scaling in small-world resistor networks. Physics Letters A 350 (5-6), 324–330.
Kozyreff, G., Vladimirov, A. G., Mandel, P., 2000. Global coupling with time delay in an array of semiconductor lasers. Physical Review Letters 85 (18), 3809–3812.
Kuramoto, Y., 1975. Self-entrainment of a population of coupled non-linear oscillators. In: Araki, H. (Ed.), Int. Symposium on Mathematical Problems in Theoretical Physics. Vol. 39 of Lecture Notes in Physics. Springer, pp. 420–422.
Kuramoto, Y., 1984a. Chemical Oscillations, Waves, and Turbulence. Springer.
Kuramoto, Y., 1984b. Cooperative dynamics of oscillator community. Progress of Theoretical Physics Supplement 79, 223–240.
Kuramoto, Y., 1991. Collective synchronization of pulse-coupled oscillators and excitable units. Physica D: Nonlinear Phenomena 50 (1), 15–30.
Leonard, N. E., Shen, T., Nabet, B., Scardovi, L., Couzin, I. D., Levin, S. A., 2012. Decision versus compromise for animal groups in motion. Proceedings of the National Academy of Sciences 109 (1), 227–232.
Lin, Z., Francis, B., Maggiore, M., 2007. State agreement for continuous-time coupled nonlinear systems. SIAM Journal on Control and Optimization 46 (1), 288–307.
Lindsey, W. C., Ghazvinian, F., Hagmann, W. C., Dessouky, K., 1985. Network synchronization. Proceedings of the IEEE 73 (10), 1445–1467.
Liu, C., Weaver, D. R., Strogatz, S. H., Reppert, S. M., 1997. Cellular construction of a circadian clock: period determination in the suprachiasmatic nuclei. Cell 91 (6), 855–860.
Lohmiller, W., Slotine, J.-J. E., 1998. On contraction analysis for non-linear systems. Automatica 34 (6), 683–696.
Lunze, J., 2011. Complete synchronization of Kuramoto oscillators. Journal of Physics A: Mathematical and Theoretical 44, 425102.
Lunze, J., 2012. Synchronization of heterogeneous agents. IEEE Transactions on Automatic Control 57 (11), 2885 –2890.
Maistrenko, Y. L., Popovych, O. V., Tass, P. A., 2005. Desynchronization and chaos in the Kuramoto model. In: Chazottes, J.-R., Fernandez, B. (Eds.), Dynamics of Coupled Map Lattices and of Related Spatially Extended Systems. Vol. 671 of Lecture Notes in Physics. Springer, pp. 285–306.
Mallada, E., Tang, A., Jun. 2010. Synchronization of phase-coupled oscillators with arbitrary topology. In: American Control Conference. Baltimore, MD, USA, pp. 1777–1782.
Mallada, E., Tang, A., Dec. 2011. Distributed clock synchronization: Joint frequency and phase consensus. In: IEEE Conf. on Decision and Control and European Control Conference. Orlando, FL, USA, pp. 6742–6747.
Martens, E. A., Barreto, E., Strogatz, S. H., Ott, E., So, P., Antonsen, T. M., 2009. Exact results for the Kuramoto model with a bimodal frequency distribution. Physical Review E 79 (2), 26204.
Mason, O., Verwoerd, M., 2007. Graph theory and networks in biology. IET Systems Biology 1 (2), 89–119.
Mauroy, A., Sacré, P., Sepulchre, R. J., Dec. 2012. Kick synchronization versus diffusive synchronization. In: IEEE Conf. on Decision and Control. Maui, HI, USA, pp. 7171–7183.
Mauroy, A., Sepulchre, R., 2012. Contraction of monotone phase-coupled oscillators. Systems & Control Letters 61 (11), 1097–1102.
Mehta, D., Kastner, M., 2011. Stationary point analysis of the one-dimensional lattice Landau gauge fixing functional, aka random phase XY Hamiltonian. Annals of Physics 326 (6), 1425–1440.
Mesbahi, M., Egerstedt, M., 2010. Graph Theoretic Methods in Multiagent Networks. Princeton University Press.
Michaels, D. C., Matyas, E. P., Jalife, J., 1987. Mechanisms of sinoatrial pacemaker synchronization: a new hypothesis. Circulation Research 61 (5), 704–714.
Mirollo, R., Strogatz, S. H., 2007. The spectrum of the

partially locked state for the Kuramoto model. Journal of Nonlinear Science 17 (4), 309–347.

Mirollo, R. E., Strogatz, S. H., 2005. The spectrum of the locked state for the Kuramoto model of coupled oscillators. Physica D: Nonlinear Phenomena 205 (1-4), 249–266.

Mirzaei, A., Heidari, M. E., Bagheri, R., Chehrazi, S., Abidi, A. A., 2007. The quadrature LC oscillator: A complete portrait based on injection locking. IEEE Journal of Solid-State Circuits 42 (9), 1916–1932.

Mizumoto, T., Otsuka, T., Nakadai, K., Takahashi, T., Komatani, K., Ogata, T., Okuno, H. G., Oct. 2010. Human-robot ensemble between robot thereminist and human percussionist using coupled oscillator model. In: IEEE/RSJ Int. Conf. on Intelligent Robots & Systems. Taipei, Taiwan, pp. 1957–1963.

Monzón, P., Paganini, F., Dec. 2005. Global considerations on the Kuramoto model of sinusoidally coupled oscillators. In: IEEE Conf. on Decision and Control. San Diego, CA, USA, pp. 3923–3928.

Moreau, L., 2004. Stability of continuous-time distributed consensus algorithms. In: IEEE Conf. on Decision and Control. Nassau, Bahamas, pp. 3998–4003.

Moreau, L., 2005. Stability of multiagent systems with time-dependent communication links. IEEE Transactions on Automatic Control 50 (2), 169–182.

Moreno, Y., Pacheco, A. F., 2004. Synchronization of Kuramoto oscillators in scale-free networks. Europhysics Letters 68, 603.

Motter, A. E., Myers, S. A., Anghel, M., Nishikawa, T., Feb. 2013. Spontaneous synchrony in power-grid networks. Nature Physics.

Münz, U., Papachristodoulou, A., Allgöwer, F., 2009. Consensus reaching in multi-agent packet-switched networks with non-linear coupling. International Journal of Control 82 (5), 953–969.

Nabi, A., Moehlis, J., 2011. Single input optimal control for globally coupled neuron networks. Journal of Neural Engineering 8, 065008.

Néda, Z., Ravasz, E., Vicsek, T., Brechet, Y., Barabási, A. L., 2000. Physics of the rhythmic applause. Physical Review E 61 (6), 6987–6992.

Nishikawa, T., Motter, A. E., Lai, Y. C., Hoppensteadt, F. C., 2003. Heterogeneity in oscillator networks: Are smaller worlds easier to synchronize? Physical Review Letters 91 (1), 14101.

Olfati-Saber, R., 2006. Swarms on sphere: A programmable swarm with synchronous behaviors like oscillator networks. In: IEEE Conf. on Decision and Control. San Diego, CA, USA, pp. 5060–5066.

Olfati-Saber, R., Fax, J. A., Murray, R. M., 2007. Consensus and cooperation in networked multi-agent systems. Proceedings of the IEEE 95 (1), 215–233.

Osipov, G. V., Kurths, J., Zhou, C., 2007. Synchronization in Oscillatory Networks. Springer.

Ott, E., Antonsen, T. M., 2008. Low dimensional behavior of large systems of globally coupled oscillators. Chaos: An Interdisciplinary Journal of Nonlinear Science 18 (3), 037113.

Paganini, F., Lesieutre, B. C., 1999. Generic properties, one-parameter deformations, and the BCU method. IEEE Transactions on Circuits and Systems I: Fundamental Theory and Applications 46 (6), 760–763.

Paley, D. A., Leonard, N. E., Sepulchre, R., Grunbaum, D., Parrish, J. K., 2007. Oscillator models and collective motion. IEEE Control Systems Magazine 27 (4), 89–105.

Pantaleone, J., 1998. Stability of incoherence in an isotropic gas of oscillating neutrinos. Physical Review D 58 (7), 073002.

Pantaleone, J., 2002. Synchronization of metronomes. American Journal of Physics 70, 992.

Pecora, L. M., Carroll, T. L., 1998. Master stability functions for synchronized coupled systems. Physical Review Letters 80 (10), 2109–2112.

Pluchino, A., Boccaletti, S., Latora, V., Rapisarda, A., 2006a. Opinion dynamics and synchronization in a network of scientific collaborations. Physica A: Statistical Mechanics and its Applications 372 (2), 316–325.

Pluchino, A., Latora, V., Rapisarda, A., 2006b. Compromise and synchronization in opinion dynamics. The European Physical Journal B - Condensed Matter and Complex Systems 50 (1), 169–176.

Popovych, O. V., Maistrenko, Y. L., Tass, P. A., 2005. Phase chaos in coupled oscillators. Physical Review E 71 (6), 065201.

Rahman, M. M. U., Mudumbai, R., Dasgupta, S., Aug. 2011. Consensus based carrier synchronization in a two node network. In: IFAC World Congress. Milan, Italy, pp. 10038–10043.

Ren, W., Beard, R. W., Atkins, E. M., 2007. Information consensus in multivehicle cooperative control: Collective group behavior through local interaction. IEEE Control Systems Magazine 27 (2), 71–82.

Restrepo, J. G., Ott, E., Hunt, B. R., 2005. Onset of synchronization in large networks of coupled oscillators. Physical Review E 71 (3), 036151.

Restrepo, J. G., Ott, E., Hunt, B. R., 2006. Synchronization in large directed networks of coupled phase oscillators. Chaos 16 (1), 015107–015107.

Righetti, L., Ijspeert, A. J., May 2006. Programmable central pattern generators: an application to biped locomotion control. In: IEEE Int. Conf. on Robotics and Automation. Orlando, FL, USA, pp. 1585–1590.

Roberts, D. C., 2008. Linear reformulation of the Kuramoto model of self-synchronizing coupled oscillators. Physical Review E 77 (3), 031114.

Rogge, J. A., Aeyels, D., 2004. Stability of phase locking in a ring of unidirectionally coupled oscillators. Journal of Physics A 37, 11135–11148.

Rohden, M., Sorge, A., Timme, M., Witthaut, D., 2012. Self-organized synchronization in decentralized power grids. Physical Review Letters 109 (6), 064101.

Russo, G., Di Bernardo, M., Sontag, E. D., 2010. Stability of networked systems: A multi-scale approach using contraction. In: IEEE Conf. on Decision and Control. Atlanta, GA, USA, pp. 6559–6564.

Sacré, P., Sepulchre, R., 2012. System analysis of oscil-

lator models in the space of phase response curves. Available at http://arxiv.org/abs/1206.4144.
Sarlette, A., Jan. 2009. Geometry and symmetries in coordination control. Ph.D. thesis, University of Liège, Belgium.
Sarlette, A., Sepulchre, R., 2009. Consensus optimization on manifolds. SIAM Journal on Control and Optimization 48 (1), 56–76.
Sastry, S., Varaiya, P., 1980. Hierarchical stability and alert state steering control of interconnected power systems. IEEE Transactions on Circuits and Systems 27 (11), 1102–1112.
Sauer, P. W., Pai, M. A., 1998. Power System Dynamics and Stability. Prentice Hall.
Scardovi, L., Dec. 2010. Clustering and synchronization in phase models with state dependent coupling. In: IEEE Conf. on Decision and Control. Atlanta, GA, USA, pp. 627–632.
Scardovi, L., Sarlette, A., Sepulchre, R., 2007. Synchronization and balancing on the N-torus. Systems & Control Letters 56 (5), 335–341.
Schmidt, G. S., Papachristodoulou, A., Münz, U., Allgöwer, F., 2012. Frequency synchronization and phase agreement in Kuramoto oscillator networks with delays. Automatica 48 (12), 3008–3017.
Sepulchre, R., 2011. Consensus on nonlinear spaces. Annual Reviews in Control 35 (1), 56–64.
Sepulchre, R., Paley, D. A., Leonard, N. E., 2007. Stabilization of planar collective motion: All-to-all communication. IEEE Transactions on Automatic Control 52 (5), 811–824.
Sepulchre, R., Paley, D. A., Leonard, N. E., 2008. Stabilization of planar collective motion with limited communication. IEEE Transactions on Automatic Control 53 (3), 706–719.
Sepulchre, R., Sarlette, A., Rouchon, P., Dec. 2010. Consensus in non-commutative spaces. In: IEEE Conf. on Decision and Control. Atlanta, GA, USA, pp. 6596–6601.
Shim, S. B., Imboden, M., Mohanty, P., 2007. Synchronized oscillation in coupled nanomechanical oscillators. Science 316 (5821), 95–99.
Simeone, O., Spagnolini, U., Bar-Ness, Y., Strogatz, S. H., 2008. Distributed synchronization in wireless networks. IEEE Signal Processing Magazine 25 (5), 81–97.
Simpson-Porco, J. W., Dörfler, F., Bullo, F., Nov. 2012. Synchronization and power sharing for droop-controlled inverters in islanded microgrids. AutomaticaTo appear.
Skardal, P. S., Sun, J., Taylor, D., Restrepo, J. G., 2013. Effects of degree-frequency correlations on network synchronization: Universality and full phase-locking. Europhysics Letters 101 (2), 20001.
Sontag, E. D., 2010. Contractive systems with inputs. In: Willems, J. C., Hara, S., Ohta, Y., Fujioka, H. (Eds.), Perspectives in Mathematical System Theory, Control, and Signal Processing. Springer, pp. 217–228.
Strogatz, S. H., 2000. From Kuramoto to Crawford: Exploring the onset of synchronization in populations of coupled oscillators. Physica D: Nonlinear Phenomena 143 (1), 1–20.
Strogatz, S. H., 2001. Exploring complex networks. Nature 410 (6825), 268–276.
Strogatz, S. H., 2003. SYNC: The Emerging Science of Spontaneous Order. Hyperion.
Strogatz, S. H., Abrams, D. M., McRobie, A., Eckhardt, B., Ott, E., 2005. Theoretical mechanics: Crowd synchrony on the Millennium Bridge. Nature 438 (7064), 43–44.
Strogatz, S. H., Mirollo, R. E., 1988. Phase-locking and critical phenomena in lattices of coupled nonlinear oscillators with random intrinsic frequencies. Physica D: Nonlinear Phenomena 31 (2), 143–168.
Subbarao, D., Uma, R., Saha, B., Phanendra, M. V. R., 2001. Self-organization on a power system. IEEE Power Engineering Review 21 (12), 59–61.
Suykens, J. A. K., Osipov, G. V., 2008. Introduction to focus issue: Synchronization in complex networks. Chaos 18 (3), 037101–037101.
Tanaka, H. A., Lichtenberg, A. J., Oishi, S., 1997. Self-synchronization of coupled oscillators with hysteretic responses. Physica D: Nonlinear Phenomena 100 (3-4), 279–300.
Tass, P. A., 2003. A model of desynchronizing deep brain stimulation with a demand-controlled coordinated reset of neural subpopulations. Biological Cybernetics 89 (2), 81–88.
Tavora, C. J., Smith, O. J. M., 1972a. Equilibrium analysis of power systems. IEEE Transactions on Power Apparatus and Systems 91 (3), 1131–1137.
Tavora, C. J., Smith, O. J. M., 1972b. Stability analysis of power systems. IEEE Transactions on Power Apparatus and Systems 91 (3), 1138–1144.
Tilton, A. K., Hsiao-Wecksler, E. T., Mehta, P. G., Jun. 2012. Filtering with rhythms: Application to estimation of gait cycle. In: American Control Conference. Montréal, Canada, pp. 3433–3438.
Tönjes, R., 2007. Pattern formation through synchronization in systems of nonidentical autonomous oscillators. Ph.D. thesis, Universitäts Potsdam, Germany.
van Hemmen, J. L., Wreszinski, W. F., 1993. Lyapunov function for the Kuramoto model of nonlinearly coupled oscillators. Journal of Statistical Physics 72 (1), 145–166.
Varela, F., Lachaux, J. P., Rodriguez, E., Martinerie, J., 2001. The brainweb: Phase synchronization and large-scale integration. Nature Reviews Neuroscience 2 (4), 229–239.
Verwoerd, M., Mason, O., 2008. Global phase-locking in finite populations of phase-coupled oscillators. SIAM Journal on Applied Dynamical Systems 7 (1), 134–160.
Verwoerd, M., Mason, O., 2009. On computing the critical coupling coefficient for the Kuramoto model on a complete bipartite graph. SIAM Journal on Applied Dynamical Systems 8 (1), 417–453.
Verwoerd, M., Mason, O., 2011. A convergence result for

the Kuramoto model with all-to-all coupling. SIAM Journal on Applied Dynamical Systems 10 (3), 906–920.

Walker, T. J., 1969. Acoustic synchrony: two mechanisms in the snowy tree cricket. Science 166 (3907), 891–894.

Wang, W., Ghosh, B., Sep. 2007. Kuramoto models, coupled oscillations and laser networks. In: SICE Annual Conference. Kagawa, Japan, pp. 130–135.

Wang, W., Slotine, J.-J. E., 2005. On partial contraction analysis for coupled nonlinear oscillators. Biological Cybernetics 92 (1), 38–53.

Wang, Y., Doyle, F. J., 2012. Optimal phase response functions for fast pulse-coupled synchronization in wireless sensor networks. IEEE Transactions on Signal Processing 60, 5583–5588.

Wang, Y., Núñez, F., Doyle, F. J., 2012. Increasing sync rate of pulse-coupled oscillators via phase response function design: theory and application to wireless networks. IEEE Transactions on Control Systems TechnologyTo appear.

Wieland, P., 2010. From static to dynamic couplings in consensus and synchronization among identical and non-identical systems. Ph.D. thesis, Universität Stuttgart.

Wiener, N., 1948. Cybernetics; or Control and Communication in the Animal and the Machine. Wiley.

Wiener, N., 1958. Nonlinear Problems in Random Theory. MIT Press.

Wiesenfeld, K., Colet, P., Strogatz, S. H., 1998. Frequency locking in Josephson arrays: Connection with the Kuramoto model. Physical Review E 57 (2), 1563–1569.

Wiley, D. A., Strogatz, S. H., Girvan, M., 2006. The size of the sync basin. Chaos 16 (1), 015103.

Winfree, A. T., 1967. Biological rhythms and the behavior of populations of coupled oscillators. Journal of Theoretical Biology 16 (1), 15–42.

Winfree, A. T., 2001. The Geometry of Biological Time, 2nd Edition. Springer.

Wu, F., Kumagai, S., 1982. Steady-state security regions of power systems. IEEE Transactions on Circuits and Systems 29 (11), 703–711.

Wu, F. F., Kumagai, S., 1980. Limits on Power Injections for Power Flow Equations to Have Secure Solutions. Electronics Research Laboratory, College of Engineering, University of California.

Yin, H., Mehta, P. G., Meyn, S. P., Shanbhag, U. V., 2012. Synchronization of coupled oscillators is a game. IEEE Transactions on Automatic Control 57 (4), 920–935.

York, R. A., Compton, R. C., 2002. Quasi-optical power combining using mutually synchronized oscillator arrays. IEEE Transactions on Microwave Theory and Techniques 39 (6), 1000–1009.

Zhang, M., Wiederhecker, G. S., Manipatruni, S., Barnard, A., McEuen, P., Lipson, M., 2012. Synchronization of micromechanical oscillators using light. Physical Review Letters 109 (23), 233906.